

The diurnal mixed layer¹

J. Imberger

Department of Civil Engineering, University of Western Australia, Nedlands, Western Australia 6009

Abstract

Fine-scale measurements and temperature gradient microstructure data are used to describe the diurnal energetics of the mixed layer in the Wellington Reservoir in Western Australia. The data covered a morning period of solar heating, a period of severe wind mixing induced by an afternoon sea breeze, and a period of pure penetrative convection extending through most of the night. The Wedderburn number (W) ranged from a value of 0.02 at the start of the heating phase to a value of about 10 at the end of the convective period. During the intermediate strong wind period the value of W remained about 0.1; the surface wind stress induced a strong tilt of the isotherms at the base of the mixed layer. The other main parameter, the ratio of the Monin-Obukhov length to the depth of the mixed layer, ranged from about 5.0 during the morning down to 0.005 at the end of the convective period. The full range of mixed-layer deepening processes could thus be analyzed.

A simple one-dimensional integral mixed-layer model was applied to assess the importance of the temporal terms in diurnal simulations and to verify the values of the energy conversion efficiencies used in such models. Overall, the model performed extremely well; however, the results showed the need to develop parameterizations for the energetics of billowing induced by large shears across the base of the mixed layer and for the mixing accompanying upwelling.

The surface mixed layer in a lake is defined as that part of the water column immediately below the free surface, which is directly influenced by the momentum and turbulence introduced by the surface wind stress and the surface buoyancy flux. The water in the mixed layer (the epilimnion) is characterized by strong turbulence, which usually leads to a relatively constant temperature distribution. However, as will be seen later, neither the temperature nor the turbulence intensity is constant in the surface layer, and the mixed layer will be defined here as that layer which is actively turbulent.

The mixed layer is separated from the deeper hypolimnetic waters by a region of increasing density. This region can be narrow, confined to a single well defined thermal step (a thermocline) or it can be made up of many steplike structures extending over an appreciable part of the depth. A broad region containing multiple thermoclines will be called the metalimnion.

Mixed layers are also common in the atmosphere. However, there is an important difference between the two situations. The time scale h/u_* , for complete mixing across

a typical mixed layer of depth h exposed to a characteristic shear velocity u_* , is only a few minutes for the atmospheric boundary layer, whereas this mixing time in a lake is close to 20 min. Atmospheric mixed layers are thus more likely to exhibit equilibrium profiles (Monin and Obukhov 1954) than mixed layers in lakes and the ocean which constantly evolve to keep pace with changing wind stresses.

A long term program of investigation has been started at Wellington Reservoir, 160 km south of Perth in Western Australia, to measure the various mixing processes contributing to the mass and momentum fluxes in the epilimnion and the hypolimnion (Imberger in prep.). It aims to gather data that will allow the parameterization of individual processes and the determination of the statistical distribution of these processes. Such information can then be used to construct predictive simulation models. This paper deals with the behavior and evolution of the mixed layer throughout a typical late summer day. Conditions in the morning were calm and hot, leading to a general heating of the surface layer. In the afternoon a strong sea breeze deepened this surface layer and the very cold, still condition during the night removed most of the heat gained in the morning. Three well defined conditions could thus be studied. First, in the morning

¹ This work was financially supported by the Australian Water Research Council and the Australian Research Grants Scheme.

the solar input stabilized the surface layer, confining the mixed layer to the top few centimeters and allowing the water to warm by nearly 1.5°C . Second, in the afternoon the strong sea breeze with winds up to 6 m s^{-1} (at a height of 4.5 m) destroyed this surface thermal gradient, deepened the mixed layer, and severely tilted the isotherms at the base of the mixed layer. Third, a rapid drop in air temperature during the night (12°C below the temperature of the water surface) and the almost complete stillness of the air gave rise to a situation of pure penetrative convection in the earlier hours of the following morning.

The behavior of the diurnal mixed layer must be distinguished from the commonly studied seasonal mixed layer (Kraus 1977), defined as that layer extending from the surface to the region of maximum gradient in the metalimnion. In the study of seasonal mixed layers individual diurnal excursions are averaged out so that long term trends of the bulk seasonal surface layer can be determined. Imberger and Hamblin (1982) discussed the connection between the two concepts and suggested that the seasonal mixed layer may conveniently be thought of as an accumulation of past diurnal mixed-layer events—the base of the diurnal mixed layer being defined as the depth of the current surface-induced turbulent activity. This concept of superposition was tested by Strub (1983) whose measurements in Castle Lake clearly illustrate the orderly evolution of the diurnal mixed layer in direct response to the meteorological forcing.

Diurnal mixed-layer models (e.g. Rayner 1980) are also based on the assumption of superposed energies. Application of this concept to the turbulent kinetic energy equation leads to few problems since the spin up and the decay times of the turbulent field are relatively small. For weak winds or if penetrative convection dominates, Spigel (1980) has shown that seiching and entrainment at the base of the mixed layer may be decoupled. In these situations, relatively simple nonentraining models (Heaps and Ramsbottom 1966; Csanady 1972) can be used successfully to compute the response of the lake to imposed wind stresses.

To understand the response to strong

winds, Spigel and Imberger (1980) studied the interaction between mixed-layer deepening and seiching of the density structure induced by imposing a sudden wind stress. Here, the momentum present in the water may result in a longer overall time for the mixed layer to respond, and entrainment at the base of the mixed layer can lead to a redistribution of momentum in the water column, modifying the baroclinic response of the lake to the wind stress. Conversely, severe seiching introduces shear across the base of the mixed layer which generates turbulence, through shear production, enhancing the ability of the wind to deepen the mixed layer. Spigel and Imberger (1980) modeled the lake stratification with a two-layer distribution and showed that the response of the mixed layer was determined by the magnitude of the surface Richardson number Ri relative to the aspect ratio $h:L$. The Richardson number is defined as $g'h/u_*^2$, where g' is the reduced gravitational acceleration due to the density jump across the base of the mixed layer, h is the depth of the mixed layer, and L is the basin length scale in the direction of the wind. This concept was formalized by Thompson and Imberger (1980), who combined the two non-dimensional parameters to form a new dimensional group which they called the Wedderburn number, W , equal to $g'h^2/u_*^2L$ (see also Imberger and Hamblin 1982).

This classification scheme, based on the two-layer model, allowed a simple description of the response of the surface mixed layer to a suddenly imposed wind stress. For strong winds, or small depths and weak stratification [$W < 0(1)$], entrainment and mixing were shown to be severe. The base of the mixed layer was predicted to surface at the upwind end with upwelling at the upwind end as a result. The active entrainment at the base of the mixed layer was predicted to lead to deepening at a rate fast enough to prevent appreciable seiching beyond the initial tilting motion, and the dissipation at the base and at the boundaries was shown to lead to an overdamped response and recovery.

At very high wind speeds ($W \ll 1$), Thompson and Imberger (1980) and Church and Thompson (1982) showed, using nu-

merical simulations, that the naive two-layer model was no longer applicable. The difficulty was that entrainment caused the base of the mixed layer to deepen at a speed comparable to the vertical advection induced by the forced heaving. These workers confirmed the findings of Mortimer (1952) and Blanton (1973) that, for high winds, upwelling was induced at the upwind end of the lake. The circulation in the mixed layer formed a vertically divergent region at the upwind end, causing enhanced vertical mixing there. Horizontal advection in the central reaches then redistributed the upwelled water laterally across the lake. By contrast, at the downwind boundary of the lake, the simulations showed the formation of a vertically convergent flow around the thermocline. This flow maintained the sharpness and horizontality of the deepening thermocline. Additional simulations, not reported, showed that on release of the surface stress the intermediate pool of water in the upwelling area intruded laterally into the thermocline, forming a fairly wide pycnocline. Qualitatively similar results were obtained by Keulegan and Brame (1960) in a series of laboratory experiments.

Monismith (1983) has given a very detailed documentation, from laboratory experiments, of the response of both a two-layer fluid and a continuously stratified fluid over a full range of surface stresses. Overall, his results closely verify the predictions of Spigel and Imberger (1980), but he focused further attention on the build-up of horizontal density gradients in the mixed layer whenever W was $\lesssim 3$. His experiments showed the existence of a closed circulation within the mixed layer almost immediately after initiation of the surface stress. At the upwind end this circulation entrained fluid from the thermocline which subsequently mixed vertically as it turned and flowed out along the surface. The upwelling and subsequent vertical mixing thus set up horizontal gradients in the mixed layer that intensified with increasing wind speed. Only at very high wind speeds did horizontal mixing prevent continued intensification of these horizontal gradients. The initial thermocline tilt and the subsequent over-damped decay, with the associated meta-

limnetic intrusions, were all observed, in agreement with the numerical simulations of Thompson and Imberger (1980).

The above results confirmed much of the qualitative picture proposed by Wedderburn (1912) for Loch Earn and by Mortimer (1952) from measurements in Windermere.

Many critical questions remain to be answered. For the case of strong winds, can the dynamics of the mixed layer be described independently of the details of the seiching motion in the lake as a whole, and is the response of the surface mixed layer and whole lake strongly damped? Does a small Wedderburn number, achieved through very small mixed-layer depth during the heating phase, lead to billowing and upwelling even at quite moderate wind speeds? Does the upwelling associated with strong tilting of the mixed-layer base lead to intrusions resulting in enhanced average net entrainment and to a broadening of the diurnal thermocline? Are the commonly used efficiencies of the turbulent kinetic energy conversion at the base of the mixed layer, derived mainly from atmospheric and laboratory experiments, applicable to the diurnal mixed layer in a lake? Is it necessary in a diurnal simulation to take into account the increases and decreases of the turbulent kinetic energy store in the mixed layer, or do simple relationships, transferring the surface inputs to the base of the mixed layer, suffice as they do for the atmosphere? Do simple equilibrium relationships apply to a diurnal mixed layer in a lake under either constant wind stress or constant heat loss? Finally, is it valid, as assumed in most mixed-layer models, to separate the sources of turbulent kinetic energy production into a region near the water surface and one at the base of the mixed layer?

The field program described below allowed the formulation of answers to many of these questions. The simulation model developed by Rayner (1980) was used to investigate the validity of the energy conversion efficiencies, and measurements of dissipation in the water column allowed direct comparison between model values and those measured in a developing diurnal mixed layer.

I thank R. Chapman for assistance with

instrumentation and D. Pullin for implementing much of the software used in the data analysis. J. Brubaker developed the earlier version of the microstructure capability and also took part in the fieldwork. D. Luketina adapted the microstructure software to allow on-line processing and also wrote most of the displacement scale code used to analyze the fine-scale casts. Much of the early development of the *Djinnang* was done in collaboration with J. Patterson. The contouring software was written by G. Prince and the *Djinnang* is maintained by K. Bentley and B. Sambell. S. Monismith, J. Patterson, G. Parker, E. Wolanski, and the reviewers made suggestions which led to improvements in the manuscript. The first draft of this manuscript was written while I was a visitor at the University of Karlsruhe.

Instrumentation and field program

A meteorological station was mounted on a spar buoy arrangement and moored in the central channel near the middle of the Wellington Reservoir (see Fig. 1). The sensor array, 4.5 m above the water surface, included three propeller anemometers to measure the u , v , and w components of the wind velocity, a Matrix Sol-a-Meter to measure the incoming beam and diffuse short-wave radiation, a Schenk net radiometer, a Väisälä humidity probe, and a thermistor to record the air temperature. All the data were acquired at a frequency of 1.67 Hz and then averaged over 10 min in an in situ logger (Univ. W. Aust. Environ. Dyn. Rep. ED-82-017).

The RV *Djinnang* was equipped with a position-fixing system, an acoustic-imaging system, a conductivity-temperature-depth system (CTD), two temperature gradient microstructure vehicles, and a data acquisition and processing facility centered around the HP 1000 minicomputer (Univ. W. Aust. Environ. Dyn. Rep. ED-83-059, ED-83-039).

The acoustic-imaging system (see Thorpe and Brubaker 1983) could resolve changes in acoustic impedance within the water column. Measurable reflections were obtained from air bubbles, clay particles, organisms, and density microstructure generated by the

turbulent fields. This information was collected as a digital time series with simultaneous display on a paper strip-chart fine-line recorder and a digital color screen. The imaging system was used to obtain synoptic information on the general activity in the water column, allowing optimum deployment (in space and time) of the fine-scale and microstructure instruments. The CTD (Univ. W. Aust. Environ. Dyn. Rep. ED-83-039) was based on the Sea-Bird temperature and conductivity sensors and deployed in three modes. First, the boat was anchored and the sensor dropped in a free-fall mode with data being acquired at a depth interval of 0.04 m (FD files), or as a 30-Hz time series (FV files). Second, the profiler was positioned at a particular depth in the water column and then towed in a horizontal plane (FT files); this allowed construction of horizontal contours of temperature, salinity, and density. Third, the boat was moved slowly with the profiler being raised and lowered in Yo-Yo fashion, acquiring data as a time series (FY files). These time series were used to construct vertical sections of the fine-scale structures, allowing resolution of small-scale features extending over only tens of meters.

The microstructure instruments were patterned on one developed by Caldwell and Dillon (1981) and much of the same software was utilized to compute the spectral properties of the temperature gradient fluctuations. In operation, this instrument glided downward and away from the vessel on release. When the desired depth was reached, a weight was jettisoned from the profiler, drag flaps were deployed, and the instrument rose vertically at about 0.1 m s^{-1} until the sensor actually pierced the water surface. The digital data were recorded at 100 Hz and the signal response was enhanced through filtering to yield a frequency resolution to 45 Hz. The data were stored on disks labeled as microstructure files (MT files).

Water velocities were estimated by tracking two wind-blind drogues, one near the surface ($0.5 \rightarrow 2.5 \text{ m}$) and the other in deeper water ($7.0 \rightarrow 9.0 \text{ m}$).

The 4-day field program began on 11 March 1982. However, the data described

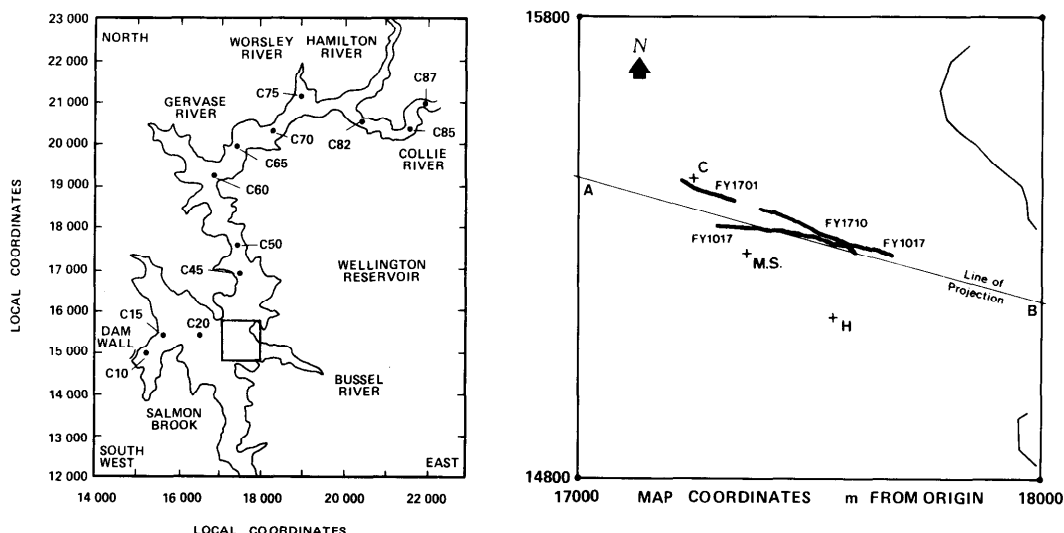


Fig. 1. Study site showing the position of the meteorological station (M.S.), the location of the data tracks, and the positions of the extra data casts (C and H). A-B is the line of projection for data presented in Fig. 9.

here are confined to the period from 0958 hours on 13 March to 0630 hours on 14 March. The data casts are detailed in Table 1 and the paths along which the FT and FY files were collected are shown in Fig. 1.

The parameter set

The influences which determine the behavior of the diurnal mixed layer can best be discussed by defining the relevant dimensionless groups governing the processes therein. The vertical thermal structure normally present in a lake during the summer season has three major features (Fig. 2) (Imberger and Patterson 1980). First, there is the deep seasonal thermocline. Second, above this is the metalimnion made up of a series of thermoclines formed during deepening events over the previous days. On a cooling phase there is usually only one such thermocline, but when the lake is progressively heating, many such thermoclines may be found, each the result of a previous penetrative convection episode. The third characteristic is the uppermost thermocline formed during midday heating and eroded as day progresses into night. This temperature gradient region is defined as the diurnal thermocline; it is the behavior of the water layer above this thermocline—the

diurnal mixed layer—which is the subject here.

Suppose that the temperature difference across the diurnal thermocline is $\Delta\theta(\text{°C})$ and a coordinate system is introduced as shown in Fig. 2. Further, suppose that at time t_0 a wind stress, τ , is imposed at the water surface. Any mechanical property R of the water column in the diurnal mixed layer will thus be given by the general relationship:

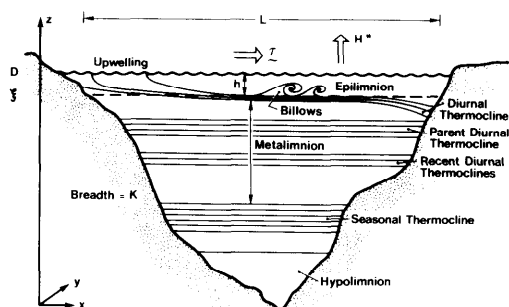


Fig. 2. Schematic showing the water column structure: D —depth; K —breadth; L —length; h —depth of diurnal mixed layer; τ —surface wind stress; H^* —net surface heat flux. The epilimnion is the turbulent surface layer. The metalimnion is defined as the layer of water from the diurnal thermocline to the deepest well defined gradient region. This layer may contain many generations of diurnal thermoclines. The hypolimnion is defined as the water below the metalimnion.

Table 1. Experimental program.

File/time*	Depth (m)	Sta.	Remarks
0958	Surface	M.S.	Surface temperature measured
EC 1011	0 → 30	—	East to west acoustic image
FY 1017	0 → 15		East to west Yo-Yo
FT 1125	0.08	Study area	Surface tow
FD 1320	22	M.S.	Wind commenced
MT 1403	7	M.S.	First microstructure profile
MT 1440	7	M.S.	
MT 1444	8	M.S.	
MT 1450	10	M.S.	
MT 1456	10	M.S.	
FD 1506	19	M.S.	Wind strength increasing
FT 1515	0.4	Study area	Surface tow
FD 1620	22	H	Cast in warm surface water
FD 1624	18	C	Cast in cold surface water
FD 1631	21	M.S.	Wind at its maximum
1635			Drogue positions noted
FY 1701	0 → 8		Yo-Yo to determine thermocline tilt
EC 1709	0 → 30		
FY 1710	0 → 8		Yo-Yo
1727			Drogue position noted
1744			Drogue position noted
MT 1748	6	C	
MT 1756	6	C	
1802			Drogue position noted
MT 1806	6	H	
MT 1809	6	H	
1816			Drogue position noted
FT 1841	0.5	West → east	Tow across study area
1853			Drogue position noted
FD 1901	23	M.S.	
MT 1908	7	M.S.	
MT 1914	7	M.S.	
FD 2247	22	M.S.	Wind had subsided
FT 2315	0.4	East → west	Linear surface tow into Study Creek
FD 0330	28	M.S.	Start of convection work
MT 0409	7	M.S.	Strong convection
MT 0413	7	M.S.	
MT 0419	7	M.S.	
MT 0423	7	M.S.	Heavy fog set in
FD 0428	27	M.S.	
FD 0445	10	M.S.	
FD 0447	10	M.S.	
FD 0449	10	M.S.	
FD 0450	10	M.S.	
FD 0451	10	M.S.	
MT 0455	7	M.S.	Weak convection
MT 0459	7	M.S.	
MT 0504	7	M.S.	
FD 0510	10	M.S.	
FT 0529	0.4	M.S.	Fog clearing
MT 0609	7	M.S.	
MT 0613	7	M.S.	
MT 0617	7	M.S.	Sun beginning to rise
MT 0621	7	M.S.	
FD 0627	10	M.S.	
FD 0628	10	M.S.	
FD 0629	10	M.S.	End of convection work

* The file names are interpreted as follows: The first letter designates the instrument (E—echo sounder; F—fine-scale CTD; M—microstructure vehicle) and the second letter is used to specify the acquisition mode (C—acoustic time series, D—depth condition channel; T—time conditional channel; Y—Yo-Yo time series). Digits specify the time of initiation of the file.

$$R = R(R_0, z, t, H^*, \tau, h, D, L, K, \nu, g, \kappa, \rho_o, \alpha, C_p, \Delta\theta), \quad (1)$$

where ν is the kinematic viscosity ($\text{m}^2 \text{s}^{-1}$), g is the acceleration due to gravity (m s^{-2}), κ is the diffusivity of heat ($\text{m}^2 \text{s}^{-1}$), ρ_o is the mean density of water (kg m^{-3}), α is the coefficient of expansion ($^\circ\text{C}^{-1}$), C_p is the specific heat of water ($\text{J kg}^{-1} \text{C}^{-1}$), H^* is the effective heat flux (W m^{-2}), R_0 is the specified initial state, and the parameters h , D , L , and K determining the geometry of the lake are defined in Fig. 2.

The heat flux H^* contributes both to the thermal energy budget of the mixed layer and separately to the mechanical balance given by Eq. 1. The effective surface heat flux, H^* , relevant to the mechanical energy equation is defined as (Kim 1976; Rayner 1980)

$$H^* = \rho_o C_p \langle w' \theta'(D) \rangle + q(D) + q(\xi) - \frac{2}{h} \int_{\xi}^D q(z) dz, \quad (2)$$

where $\rho_o C_p \langle w' \theta'(D) \rangle$ is the surface heat flux, $q(D)$ is the net radiation at the surface, $q(z)$ the radiation in the water column at a height z , and $q(\xi)$ is the radiation remaining at the base of the mixed layer.

Equation 1 can be simplified because the surface stress, τ , only enters the equations of motion as the quotient τ/ρ_o . This suggests that τ may be replaced by the variable

$$u_* = \left(\frac{\tau}{\rho_o} \right)^{1/2}, \quad (3)$$

the surface water shear velocity (m s^{-1}). Similarly, since R is a mechanical and not a thermal property of the fluid, the effective heat flux, H^* , only enters Eq. 1 through the buoyancy flux B ($\text{m}^2 \text{s}^{-3}$), defined as

$$B = \frac{g \alpha H^*}{C_p \rho_o}. \quad (4)$$

It is further convenient, by analogy with the definition of the shear velocity, to introduce the penetrative convection velocity scale (Deardorff 1970):

$$w_* = (Bh)^{1/2}. \quad (5)$$

The temperature differential, $\Delta\theta$, again,

cannot enter a mechanical equation in isolation but only in combination with α and g , so it is usual to introduce the modified acceleration due to gravity,

$$g' = \alpha \Delta\theta g, \quad (6)$$

which basically represents the weight difference across the diurnal thermocline.

If we neglect the barotropic response of the lake, the quantities α , g , C_p , and ρ_o only enter through the variables defined in Eq. 3–6. Equation 1 can thus be rewritten as

$$\frac{R}{R_0} = R(z, t, u_*, w_*, h, L, D, K, \nu, \kappa, g'). \quad (7)$$

Dimensional analysis suggests that there are nine dimensionless groups. It is useful to choose these groups as follows, so that each has a dynamical significance.

$\frac{hw_*}{\nu}$: Reynolds number relevant to turbulence maintained by penetrative convection. Often this group is retained as the cube of the quantity, given by Bh^4/ν^3 , which is the Grashoff number.

$\left(\frac{u_*}{w_*} \right)^3$: The ratio of the rate of turbulent kinetic energy generated by the surface wind stress to that introduced or drained by the mechanical equivalent of the surface thermal flux. A positive heat flux, corresponding to a surface heating, leads to a positive value representing the ratio of the wind energy input to the rate of gain of potential energy arising from the heating at the surface. It is usual to introduce the Monin-Obukhov length, l , defined (Monin and Obukhov 1954) by

$$l = \frac{u_*^3}{B}. \quad (8)$$

In terms of l , the ratio becomes l/h . For a net surface heat input (H^* positive), the length l represents the depth scale over which wind stirring roughly balances the rate of gain of potential energy from the surface heating. On the other hand, for a heat loss (H^* negative) l is negative and l/h represents that fraction of the mixed-layer depth influenced by u_* ; below the depth l , penetrative convection dominates (Kaimal et al. 1976) the turbulence field.

$\frac{g'h}{u_*^2} \times \frac{h}{L}$: The ratio of the maximum baroclinic pressure force (before the upwind surfacing of the diurnal thermocline) and the surface wind force. This ratio was first introduced by Spigel and Imberger (1980) and has been called the Wedderburn number, W , by Thompson and Imberger (1980). The magnitude of W determines the deepening regime of the diurnal mixed layer.

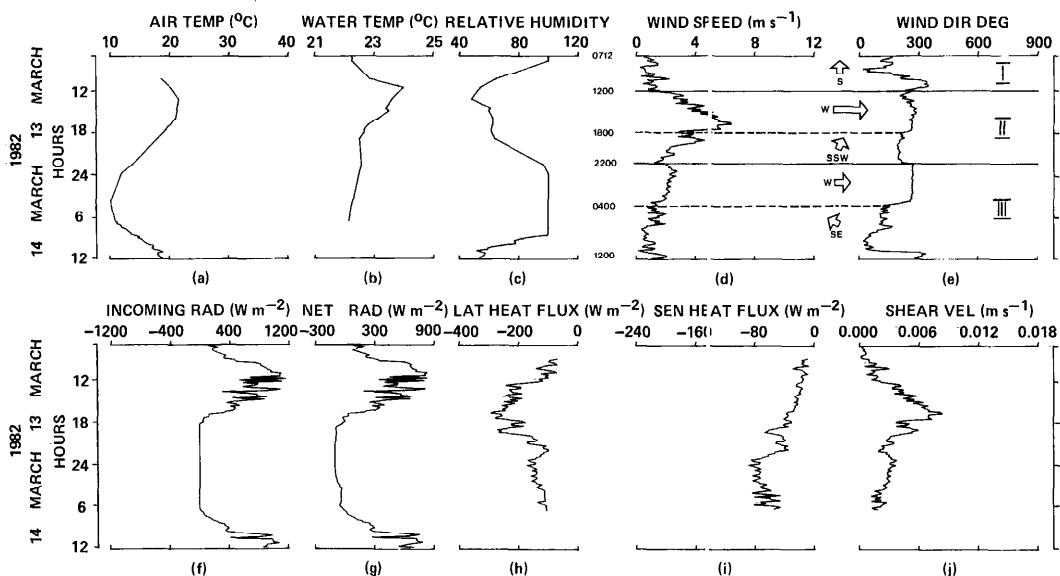


Fig. 3. Meteorological variables at 4.0 m and the derived fluxes vs. time of day. The fluxes were computed allowing for the stability of the atmospheric boundary layer. Relative humidity (c) is % saturation; wind direction (e) is degrees measured from north.

$\frac{h}{D}$: Aspect ratio of the diurnal mixed layer. During any severe wind event, the diurnal mixed layer quickly deepens to the parent thermocline, leading to a basically three-layer system, partitioned by the parent and the seasonal thermoclines. The depth of the seasonal thermocline usually varies only, as the name implies, on a seasonal time scale, and so the aspect ratio determines the whole basin response to a diurnal wind.

$\frac{D}{L}, \frac{K}{L^2}$: Aspect ratios determining the lake geometry.

$\frac{hw_*}{\kappa}$: The Peclet number, important in the details of penetrative convection process (Denton and Wood 1981).

$\frac{z}{h}, \frac{tu_*}{h}$: Dimensional depth and time scales, defined as mixed-layer variables and not surface variables.

For any particular lake, the geometric aspect ratios are more or less fixed and, in our case, they are very small. Thus for a particular study, it is possible to simplify Eq. 7 to read:

$$\frac{R}{R_0} = f \left(\frac{z}{h}, \frac{tu_*}{h}, \frac{l}{h}, W, \frac{hw_*}{\nu}, \frac{h}{D}, \frac{hw_*}{\kappa} \right). \quad (9)$$

The experimental data described in the next sections allowed an examination of a number of properties R of the mixed layer over a wide range of the variables z/h , tu_*/h , l/h , and W . The variable hw_*/ν is retained in Eq. 9 so that ν is available for the law-of-the-wall scaling at the higher wind speeds. The dynamic response ratio $h:D$ was fixed by the basin stratification and did not vary much. Similarly, the Peclet number, important during the convective period, was almost constant throughout that time.

Meteorological forcing

Conditions on the morning of 13 March, at the start of the experiment, were warm and sunny, with only a weak wind rippling the water surface. At noon the air temperature reached a peak of 21.6°C . A southwesterly sea breeze began shortly after midday (Fig. 3d, e) and intensified throughout the afternoon until at 1648 hours it reached a peak speed of 6.5 m s^{-1} , leading to strong wave action on the water surface and gusty conditions over most of the central basin. Toward evening the wind decreased and the air temperature dropped dramatically, until at midnight there was a temperature differ-

ence of 12°C between air and water. This large temperature difference and the low wind led to a sharper rise in humidity, saturating the air and bringing about dense fog over most of the lake. This fog did not clear until about 0800 hours on 14 March.

The corresponding air-water heat fluxes are shown in Fig. 3f-i. The short-wave and total net wave radiation were measured directly at the site. The peak solar input reached about $1,100 \text{ W m}^{-2}$ at noon, but clouds interrupted the radiation flux in the afternoon. The net flux, a measure of both short- and long-wave radiation, rose to about 800 W m^{-2} at midday and then decreased, reaching zero just before sunset. At midnight the net radiation flux had reversed and reached a minimum of around -100 W m^{-2} , but this strong outward loss decreased to about -30 W m^{-2} around 0400 hours on 14 March as the fog intensified.

The latent and sensible heat fluxes and the surface shear velocity were calculated from bulk aerodynamic formulae (see Fischer et al. 1979) with the exchange coefficients corrected for the stability of the air column by the procedure of Hicks (1975). An algorithm developed initially by Rayner (1980) was modified and applied to the meteorological data. The drag and exchange coefficients varied considerably over the day, with morning and night values of the drag coefficient typically around 1.8×10^{-3} but decreasing to neutral values of around 1.3×10^{-3} during the high wind in the afternoon. The resulting fluxes and water shear velocity are shown in Fig. 3h-j.

Both the sensible and latent heat fluxes were outward, and thus negative, during the study, but the contribution from the sensible flux was quite small, except for the late night and early morning periods when it became comparable to the latent heat flux. During the windy afternoon period (1200–2300 hours), the latent heat flux reached a minimum value of -225 W m^{-2} , but the magnitude of the sensible heat loss was $< 20 \text{ W m}^{-2}$. The morning hours of 14 March were marked by two distinct periods of near constant surface heat fluxes. The first occurred between 2300 hours on 13 March and 0200 hours on 14 March when the sensible heat flux average was -75 W m^{-2} ,

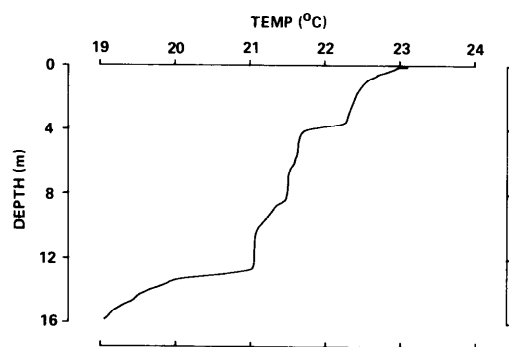


Fig. 4. Temperature vs. depth at the meteorological station at the start of study period at 1017 hours. The profile is the average of five downward legs of the Yo-Yo trace shown in Fig. 5. A new diurnal thermocline is seen to have formed around the 1-m mark. The parent thermocline was located at about 3.5 m deep, with further well defined gradient regions at 8.3 and 12.6 m.

latent heat flux -145 W m^{-2} , and the net radiation -95 W m^{-2} , yielding an average net heat loss from the water surface of 314 W m^{-2} . The second period began at about 0400 hours and continued until about 0630 hours. During this time the radiation flux was steady at -27 W m^{-2} , the latent heat flux at -111 W m^{-2} , and the sensible heat flux at -62 W m^{-2} , giving a net average heat loss of about 200 W m^{-2} from the water surface.

The shear velocity variation induced by the wind (Fig. 3j) reached a peak of around 0.008 m s^{-1} at 1648 hours. The wind then decreased and essentially ceased by about 2300 hours.

The water temperature variation is shown in Fig. 3b. The expected effects of the surface fluxes are clearly visible. The morning heating led to a general warming of the water surface to 24°C . The commencement of the wind at noon deepened the structure, decreasing the surface water temperature to 22.5°C by 1914 hours. However, the temperature increased slightly again during the 3.5 h immediately following this minimum. This increase could have been due only to advection into the measuring site, since the net heat flux was outward for the whole period. From 2300 hours onward, the water surface cooled continuously, reaching a minimum of 22.1°C at 0600 hours on 14 March.

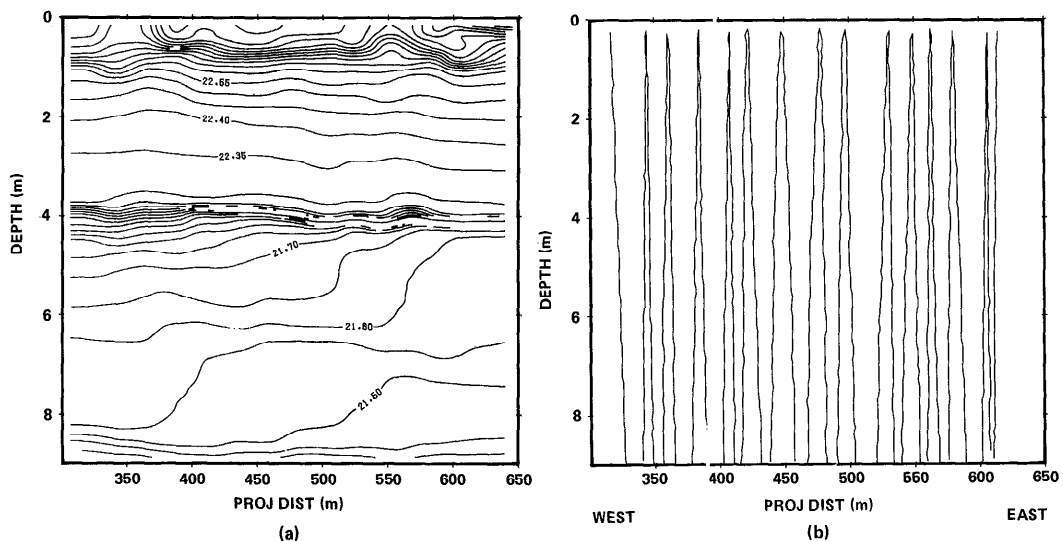


Fig. 5. Isotherm contours for the file FY 1017. The horizontal path of the transect is shown in Fig. 1 and the origin of the transect is point A (17,000, 15,450). The projection is onto the line A-B and the trace included 15 legs of the Yo-Yo. Particularly noticeable is the overturning event in the mixed layer at the 350- and 600-m marks. The parent thermocline showed a definite variation in structure from east to west with a marked intensification of the thermocline near 600 m.

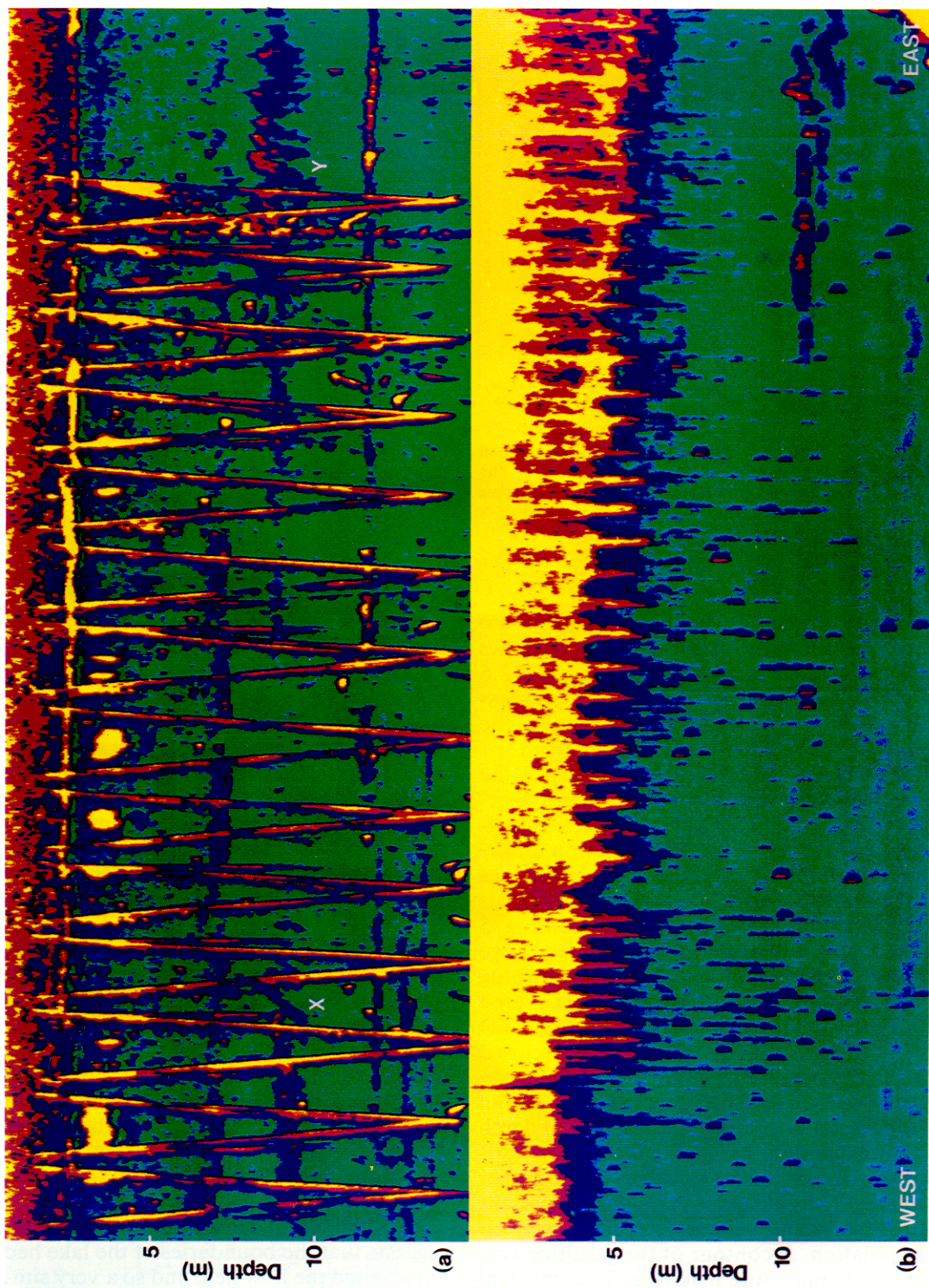
Morning heating—Period 1

The first CTD cast, a Yo-Yo time series, was made at 1017 hours (see Fig. 1). Five consecutive downward legs of the FY file, opposite the weather station, were isolated and averaged to produce a mean temperature profile (Fig. 4). Contours derived from the total FY file over the first 9 m of the water column are shown in Fig. 5. At the time the data were gathered a weak westerly breeze had sprung up, with a maximum speed of about 2.0 m s^{-1} (see Fig. 3d). However, this wind lasted for only about 20 min,

and it did not interrupt the general heating during the morning.

Figures 4 and 5 show that the generally calm conditions, together with the strong and increasing solar insolation, led to a four-layer structure. The seasonal thermocline was at about 13.0 m (Fig. 4). Above this there was a weak secondary thermocline at 8.5 m, and a much stronger thermocline remained from the previous evening at 3.5 m. The presence of these intermediate elevated thermoclines indicates that the lake was warming at the time.

Fig. 6. a. Acoustic image accompanying the temperature field shown in Fig. 5a. The regular vertical Yo-Yo pattern is the image of the CTD profiler itself. Particularly noticeable is the activity in the diurnal gradient region down to 3.0 m. The reflections are intermittent and are most likely concentrations at zooplankton and weak turbulent patches. The parent thermocline of 3.5 m is clearly marked by a strong reflection as are the gradient regions at 8.3 and 12.6 m. At the points X and Y the image shows clear evidence of roll-type overturning events. The weak density gradients were obviously insufficient to prevent any small residual seiching motion from causing local overturning. b. Acoustic image accompanying the temperature field shown in Fig. 11a. The Yo-Yo profile extended only to a depth of about 7 m as seen in Fig. 11b. The base of the mixed layer is clearly distinguishable between the CTD tracks and shows the same heaving as the thermocline in Fig. 11a. The image in the mixed layer was much more intense than that in Fig. 6a even with the digital gain reduced by a factor of 4. Further, the overall intensity is more uniform in the production regions near the surface and at the mixed-layer base. The structure below the mixed layer is somewhat obscured due to the small gain and because of the increased noise from wave activity at the surface in the image.



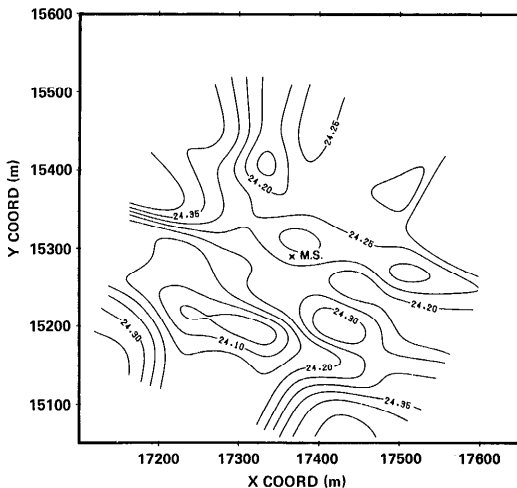


Fig. 7. Contours of the horizontal temperature field at a depth of 0.08 m throughout the study area. The data have been corrected for sensor elevation changes by multiplying the sensor depth deviation from 0.08 m by the local vertical temperature gradient ($10^{\circ}\text{C m}^{-1}$). Little systematic temperature structure is observable.

The enhanced acoustic image (Fig. 6a) corresponding to the FY file clearly shows the three thermoclines at 3.5, 8.3, and 12.6 m. Two distinct sets of billows are also visible, both around the 10-m mark, one at the start of the transect and one at the end.

The strong gradient region between the water surface and the 3.5-m parent thermocline exhibited a patchy reflection pattern, probably due to a combination of turbulence induced by the wind, air bubbles (Thorpe 1984), and floating particulate matter. The turbulence is also evident in Fig. 5 where the isotherms show relatively large displacements with associated overturning near the surface. At 1125 hours, we covered the experimental area by towing the CTD at a constant depth of 0.08 m around a closed grid. Conditions were calm with a glassy water surface so that a successful tow could be completed at this shallow constant depth without contaminating the signal with variations due to vertical motions of the sensor package. Any effects of very slight variations of sensor depth were removed by linear interpolation. A contour of the resulting corrected temperature field (Fig. 7) shows that the surface water was essentially uniform at 24.2°C , with a weak depression just south-

west of the meteorological station. Heating was obviously proceeding at a uniform rate over most of the lake surface.

To evaluate the variations of the nondimensional parameters in Eq. 9 we must choose an effective mixed-layer depth from the data and an effective basin length for an equivalent two-dimensional rectangular system. The difficulty of estimating these two length scales from field data is fully discussed by Patterson et al. (1984). The main difficulty is that the dynamic response of a many-layered system (Fig. 4) in an irregular basin is to be compared with that of a two-layered system in a rectangular tank. However, Monismith (1985) showed that the shear across the base of the surface mixed layer is completely dominated by the second internal wave mode, so that it is appropriate to choose the mixed-layer depth h as the vertical length scale and L , the basin width, as the horizontal length scale when computing the Wedderburn number.

Table 2 gives the values of the various nondimensional parameters in Eq. 9. At 1017 hours, the Monin-Obukhov length in the water column was -2.5 m, indicating an effective heat loss from the surface of the mixed layer. The Wedderburn number for the same period was 0.02, a very small value. The large negative Monin-Obukhov length and the small Wedderburn number together indicate that mixing was essentially sustained by surface wind production and shear production at the base of the mixed layer. The gain in potential energy, due to the strong solar heating, appeared to cancel the energy input from natural convection driven by the net surface heat losses, so that H^* , the effective surface heat loss entering the mechanical energy balance, was only -11 W m^{-2} . The turbulent kinetic energy balance thus maintained a shallow mixed layer which allowed the thermal fluxes (thermal budget) to steadily raise the surface temperature to 24.1°C by noon (Fig. 7) without, however, further shallowing the mixed layer.

The horizontal nature of the isotherms suggests that the boundaries of the lake had not affected the flow field and so a very simple momentum balance (Spigel and Imberger 1980),

Table 2. Values of experimental parameters. Coefficient of expansion $\alpha = 2.54 \times 10^{-4} \text{C}^{-1}$; solar radiation penetration $q(D) = q(D)\{A_1 \exp[-\beta_1(D - z)] + A_2 \exp[-\beta_2(D - z)] + A_3 \exp[-\beta_3(D - z)]\}$, with assumed values $A_1 = 0.42$, $A_2 = 0.42$, $A_3 = 0.42$, $\beta_1 = 0.16$, $\beta_2 = 0.9$, $\beta_3 = 6.9$. $\beta_1 = 0.9$, $\beta_2 = 6.9$, $\beta_3 = 69.0$ chosen as discussed in model section; specific heat $C_p = 4,180 \text{ J kg}^{-1} \text{C}^{-1}$; and length $L = 1,800 \text{ m}$.

Time (hours)	h (m)	h^* ($\times 10^{-3}$ m s $^{-1}$)	$\Delta\theta$ (°C)	g' ($\times 10^{-3}$ m s $^{-2}$)	$-B$ ($\times 10^{-7}$ m 2 s $^{-3}$)	$-I$ (m)	$\frac{h}{w^*}$ ($\times 10^{-3}$ m s $^{-1}$)	$\frac{h}{w^*}$ ($\times 10^3$ s)	$\frac{h}{w}$	$\frac{ I }{h}$	Remarks
13 March											
1017	1	0.5	2.5	0.4	0.9	11	0.06	2.5	1.4	0.36	0.02
1320	2	0.8	3.4	1.4	3.5	168	0.91	0.5	4.2	0.20	0.04
1440/1456	2	1.7	5.5	0.8	2.0	10	0.06	27.7	2.2	0.77	0.31
1506	2	1.7	5.5	1.0	2.5	144	0.06	1.9	5.3	0.32	0.13
1631	2	4.0	7.0	1.0	2.5	110	0.66	5.2	5.4	0.63	0.57
1748/1756	2	5.1	4.0	0.6	1.5	236	1.41	0.5	8.9	0.57	1.35
1806/1809	2	6.2	3.7	0.7	1.7	206	1.16	0.4	9.0	0.69	1.67
1901	2	6.7	5.3	0.5	1.3	372	2.22	0.7	11.4	1.26	0.59
1908/1914	2	6.3	5.9	0.6	1.5	413	2.31	0.9	11.3	0.56	1.07
2247	3	3.74	2.9	0.1	0.3	280	1.67	0.15	8.6	0.43	1.20
14 March											
0330	3	4.75	2.5	0.2	0.5	240	1.43	0.11	8.7	0.55	1.90
0409/0423	3	5.3	2.2	0.5	1.3	216	1.29	0.08	8.8	0.60	2.41
0449	3	5.5	2.1	0.5	1.3	214	1.27	0.07	8.8	0.62	2.62
0455/0504	3	5.4	1.6	0.5	1.3	193	1.15	0.04	8.5	0.64	3.38
0609/0621	3	5.4	1.3	0.5	1.3	185	1.10	0.02	8.4	0.64	4.15
0627	3	5.6	1.5	0.5	1.3	169	1.01	0.03	8.3	0.67	3.73

$$\frac{d}{dt}(uh) = u_*^2, \quad (10)$$

suffices to estimate the surface mixed-layer velocity u . This conclusion also follows directly by noting that the quarter period of the second mode internal wave was about 3 h (Monismith 1985). Integration of Eq. 10 is simple since the average shear velocity u_* was approximately constant (1.5×10^{-3} m s $^{-1}$) for the whole morning period. The mixed-layer depth here is designated by h and the time from the commencement of the wind field by t . Further, since W was very small during this period, it can be assumed that shear production was the dominant source of turbulent kinetic energy. The simple entrainment hypothesis (Sherman et al. 1978) thus results:

$$F = \frac{u}{(g'h)^{1/2}} = C \quad (11)$$

where F is the layer Froude number, g' is the modified acceleration due to gravity ($(\Delta\rho/\rho)g$), and C is an empirically determined constant. Pollard et al. (1973) used Eq. 11 with $C = 1.0$, but only applied the criterion to mean seasonal mixed layers. Spigel and Imberger (1980) suggested a value ranging from 1.41 to 2.24. Rayner (1980) applied a similar equation to a diurnal mixed-layer data set from the Wellington and found that the best fit to his data was obtained with the upper limit of 2.24. Interpreted in terms of energy, Rayner's value is equivalent to a 20% conversion of available mean kinetic energy to potential energy associated with the deepening process. Pollard et al. (1973) used daily mean wind speeds, underestimating the rate of working, and this could explain the apparent higher utilization of energy implied by the lower value of C .

Combined, the integral of Eq. 10 and 11 allows the simple prediction for the mixed-layer depth h at time t :

$$h = \left(\frac{u_*^4 t^2}{C^2 g'} \right)^{1/3} \quad (12)$$

where $g'(t)$ is now a function of time, dependent on the immediate past history of the entrainment process, the surface heat input, and the gradient in the metalimnion.

The momentum origin ($t = 0$) may be as-

sumed as the time when the strong natural convection processes from the previous night had stopped and the surface heating had started. This occurred at about 0800 hours, giving a value for t equal to about 2.5 h for the data in Fig. 5. Substituting the average shear velocity (since the layer water velocity determines the shear) into Eq. 12 and using the value of g' listed in Table 2 for the time 1017 hours leads to a mixed-layer depth of about 0.5 m, using a value of $C = 2.24$, in good agreement with the results shown in Fig. 5. The diffuse nature of the thermocline, evident in the field data, also follows directly since shear production was a dominant source of turbulent kinetic energy. The billowing associated with such a strongly sheared thermocline was shown by Thorpe (1973) to lead to a diffuse interface of thickness δ of $O(u^2/g')$. Sherman et al. (1978) suggested the equation:

$$\delta = \frac{0.3 u^2}{g'} . \quad (13)$$

Substituting the velocity obtained from Eq. 10 and using the same value for g' leads to a thickness of 0.6 m, which is actually slightly larger than the mixed-layer depth itself. This is consistent with the diffuse active mixed layer, billowing over its entire depth, measured at 1017 hours. In Fig. 5, billow-like disturbances are evident at the 350- and 600-m transect lengths. As discussed below, surface production of kinetic energy was also a major contributor to the mechanical energy budget throughout the morning, but as suggested by Pollard et al. (1973), the depth of the mixed layer quickly adjusts to shear production whenever the momentum of the layer increases.

Sea breeze deepening—Period 2

The sea breeze began about noon (13 March) and continued until 2136 hours, reaching a peak at 1648 hours. The behavior of the water column at the weather station site is most easily displayed by a temperature-time contour plot (Fig. 8). The isotherms show the formation of a strong, shallow, diurnal thermocline during the morning heating period, with the surface temperature reaching a maximum around noon. The beginning of the wind, just after 1200 hours,

caused a rapid deepening of the mixed layer. This is evident from the slope of the isotherms in Fig. 8 and from the way the isotherms between 23.4° and 22.6°C peel off from the main thermocline and progressively surface with time. About the time of maximum wind stress (1648 hours) this slope relaxed and the rate of cooling decreased. This is particularly evident from the behavior of the 22.4°C isotherm which is at the center of the diurnal thermocline. Further, about 1 h before the wind reached its maximum, the diurnal thermocline penetrated to the parent thermocline previously lying at about 3.5 m.

The wind eased after 1648 hours, but the thermal structure continued to tilt and deepen for another 2.5 h, reaching a maximum angle at 2130 hours, by which time the thermocline had deepened at the meteorological station to about 6.0 m. After this, the structure recovered quite quickly with no overshoot, reaching its new equilibrium position at about 2245 hours, nearly 3.5 h after the time of maximum tilt. The above behavior suggests that entrainment dominated the deepening of the wind mixed layer in the early part of the wind cycle. However, Monismith (1985) noted that the quarter period of the second internal wave mode was between 2 and 3 h, so that tilting of the isotherms would have contributed significantly to the lowering of the thermocline even before the wind had reached its maximum.

It is also interesting that the rate of change of temperature in the mixed layer decreased noticeably at 1648 hours leading to the minimum temperature at 2130 hours, the time of maximum thermocline depression. During the rebound period the temperature in the mixed layer actually rose slightly before falling again under the influence of the early morning convective cooling.

The tilting and rebounding of the base of the mixed layer was also reflected in the evolution of the west–east temperature gradients of the mixed layer in the study area. Horizontal tow data projected onto the section A–B (Fig. 1) are shown in Fig. 9. The data corresponding to the first two times are projections of four legs of a horizontal tow extending over the whole study area. The

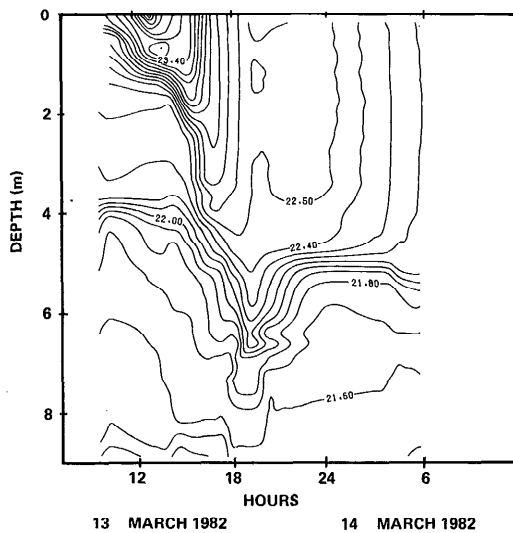


Fig. 8. Isotherms as a function of depth and time at the meteorological station. The contours were prepared from all the FD and MT files as well as the averages of the FY listed in Table 2. The contour package used a local filter to distribute the data points from the files onto a 64×64 grid. The horizontal width of the normal ellipsoidal filter was 0.67 times the spacing at the casts and 0.1 m in the vertical. The heating period lasted until about 1200 hours whereupon the sea breeze began. The wind peaked at 1648 hours heading to a maximum tilt at 1941 hours. The structure had returned to its neutral position (in an overdamped position) at 2136 hours. After this time a gradual cooling took place with a definite unstable temperature gradient near the surface.

particular legs were chosen to encompass a rough west–east coverage around the weather station. The remaining two data sets shown are linear tows in and out of Study Creek (Fig. 1). The data shown in Fig. 9 clearly illustrate the buildup of a west–east temperature gradient as the deepening progressed, the western boundary cooling slightly faster than the water in the east near the entrance of Study Creek. This suggests a tilting of the isotherms from west to east, leading to a shallower mixed layer with associated enhanced entrainment and thus colder temperatures at the western end of the study zone. At 1841 hours the temperature was patchy with strong gradients along the transect. These frontal structures had vanished, leaving a smooth temperature rise from west to east by 2315 hours, again suggesting that vertical and horizontal mixing

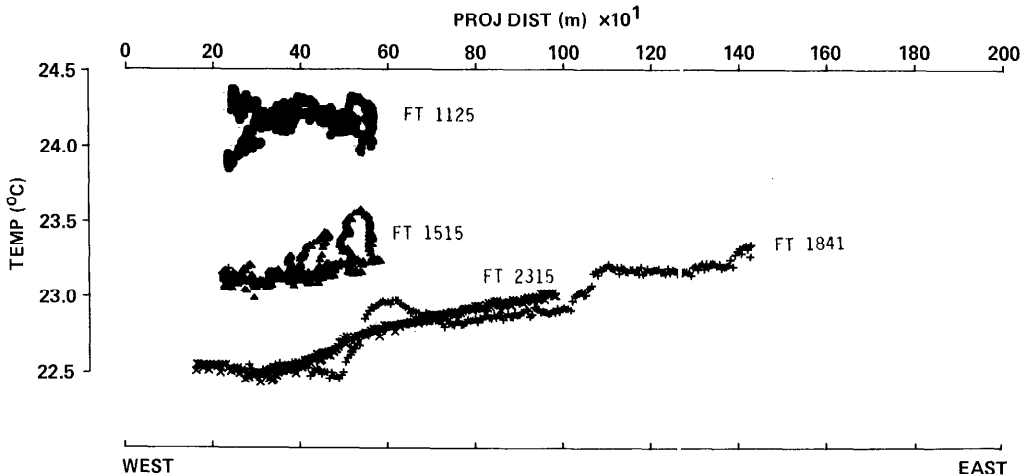


Fig. 9. Surface temperature ($^{\circ}$ C) vs. projected distance (m) along the transect A-B.

had smoothed out earlier gradients. Also noticeable from Fig. 9 is the slight rise in temperature between 1841 and 2315 hours, again implying a westward migration of the surface waters.

The buildup of a horizontal temperature gradient during the middle of the afternoon was confirmed with a horizontal tow covering the whole area at a depth of 0.4 m (Fig. 10). A relatively strong front with a temperature difference of nearly 0.4° C had formed just east of the weather station (M.S.). The direction of the front was almost

perpendicular to Study Creek, suggesting that the mixed-layer water was being banked up in the side arm formed by the creek valley.

To document the associated tilt of the isotherms in the vertical plane at the time of maximum wind strength, we began a vertical Yo-Yo section in the direction of the Study Creek entrance, parallel to the wind, at 1701 hours from a point west of the weather station (Fig. 11). The diurnal thermocline had disappeared and the parent thermocline had attained a mean tilt of about 3.6×10^{-3} ; the isotherms show evidence of a great deal of internal wave straining at scales ranging from tens of meters up to >300 m. The magnitude of the tilt and the very much increased strength of the turbulence is confirmed in the corresponding acoustic image (Fig. 6b). At the eastern end of the section, where the mixed layer is deeper, there is some evidence of a separation of the zones of turbulence production; the acoustic image shows stronger reflections near the surface and at the base of the mixed layer and somewhat weaker activity at middepth.

The tilt documented in Figs. 6b and 11 implies a mixed-layer depth at the eastern boundary near the entrance of Study Creek of about 2 m below that at the meteorological station, a distance of 580 m. The change in depth due to tilting is thus comparable to that derived from entrainment.

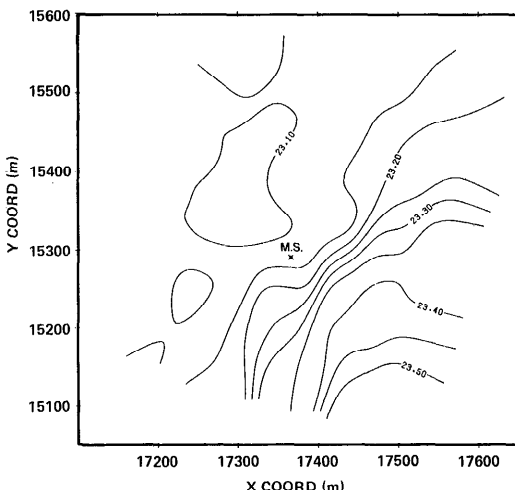


Fig. 10. Contours of the horizontal temperature field at a depth of 0.4 m.

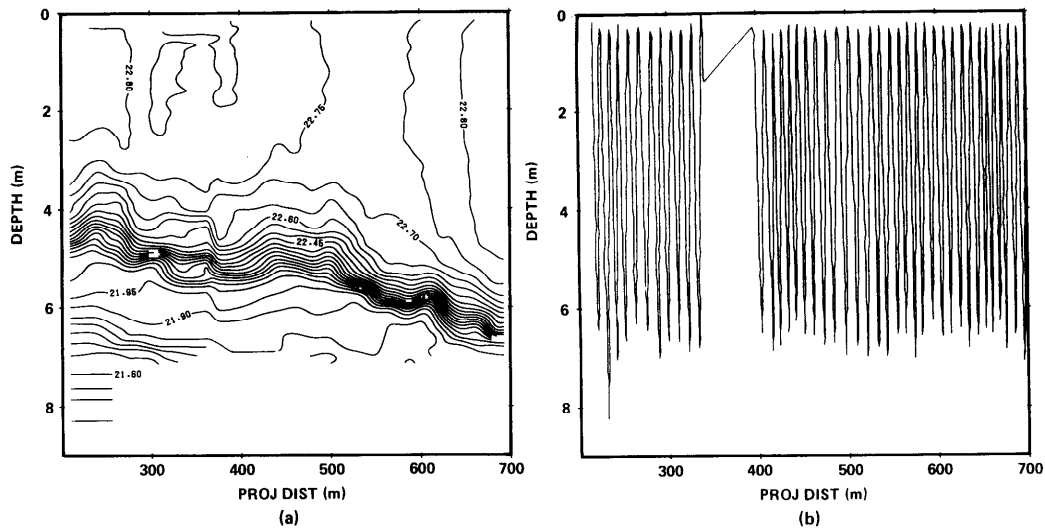


Fig. 11. Isotherm contours for the files FY 1701 and FY 1710. The path of the transect is shown in Fig. 1 and the projection is the same as that used in Fig. 5a. The contour was constructed from 42 legs of the Yo-Yo. The mean tilt of the isotherms at the base of the mixed layer is 3.6×10^{-3} .

During the time of peak wind, the velocity in the mixed layer was measured with drogues set at a mean depth of about 1.5 m. The drogues were about 2 m long and thus sampled the average velocity in the mixed layer. They were tracked continuously, being restarted every 30 or 45 min near the weather station at the times shown in Table 1. The surface water generally moved in the easterly direction with a velocity of 0.09 m s^{-1} at 1700 hours, 0.119 m s^{-1} at 1800 hours, and 0.049 m s^{-1} at 1837 hours.

Equation 10 can be used to define the major features of the deepening event. For this purpose, we assume that the shear velocity can be adequately described by the variation (Fig. 3j)

$$u_* = 1.5 \times 10^{-3}$$

$$0830 < T < 1200 \text{ hours}$$

and

$$u_* = 1.5 \times 10^{-3} + 3.75 \times 10^{-7} t$$

$$1200 < T < 1700 \text{ hours} \quad (14)$$

where t is the time in seconds after 0830 or 1200 hours, depending on which expression is used, and T is the actual time. Substituting Eq. 14 into 10 and carrying out the necessary integrations leads to an advected vol-

ume per unit width of 179 m^2 by noon and a volume of $2,860 \text{ m}^2$ by 1700 hours. Assuming a simple planar tilt thus suggests an effective basin length of $1,783 \text{ m}$ for the measured tilt of 3.6×10^{-3} . Since the lake shape is quite irregular, this length is reasonable and corresponds to 1.7 times the length of the study area shown in Fig. 1.

The other comparison afforded by this simple model is the induced mixed-layer velocity. A single integration of Eq. 10 yields a mass flux per unit width of $0.52 \text{ m}^2 \text{ s}^{-1}$ at 1700 hours, and, when combined with a mixed-layer depth of 5.0 m, this leads to a mixed-layer velocity of 0.10 m s^{-1} , in reasonable agreement with the drogue measurements.

The easterly water movement in the mixed layer must also have led to an advection of the temperature field from west to east, and this movement should be reflected in the isotherms in Fig. 10. The mixed-layer temperature at the weather station at 1506 hours was 23.45°C , but at 1530 hours had decreased to 23.12°C . The rate of decrease, due to the surface fluxes and the entrainment at the base of the mixed layer, was calculated with a numerical simulation (discussed below) and found to have the value $5.63 \times 10^{-5}^\circ\text{C s}^{-1}$. At 1530 hours the parcel

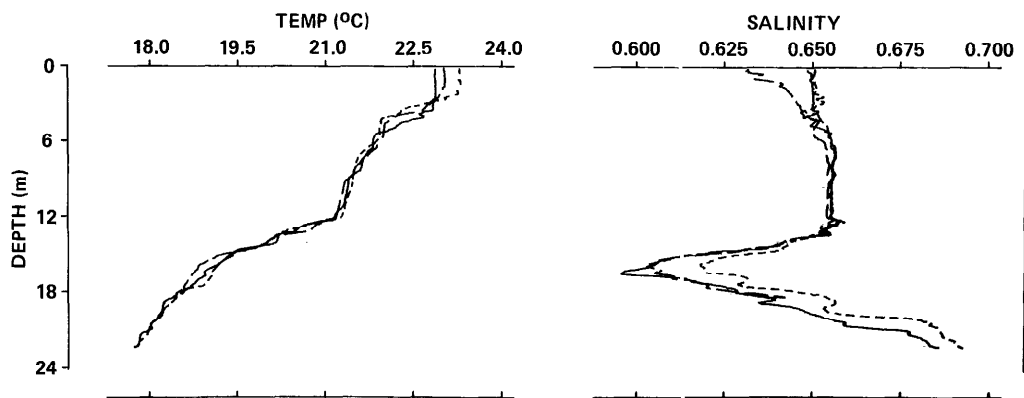


Fig. 12. Results of the CTD casts positioned across the study area. Dashed line—FD 1620 taken at sta. H; solid line—FD 1631 taken at M.S.; broken line—FD 1624 taken at sta. C. The salinity profiles show that a weak gradient existed from C to H below about 12 m.

of water originally at the meteorological station would thus have attained a temperature of 23.37°C. The isotherm corresponding to this temperature had moved about 120 m toward the southeast of the weather station in the 24 min which had elapsed. This shift is consistent with the surface drift and implies a velocity in the mixed layer of 0.08 m s⁻¹, again in good agreement with the above simple momentum model. The enhanced entrainment and mixing at the upwind, upwelling western boundary thus led to a reduced mixed-layer temperature, which was then swept east by the advection across the study site.

The horizontal advection and the for-

mation of horizontal gradients in temperature were also demonstrated with a numerical simulation by Thompson and Imberger (1980). They showed how tilting of the thermocline increased with wind speed. For a Wedderburn number of about 2, large-scale overturning was observed at the upwind end, a result verified and extended by Monismith (1983).

The changes in the temperature structure below the mixed layer must be attributed mainly to basin-scaling internal seiching, although it could be expected that some short-wavelength internal waves would have been propagating throughout the hypolimnion. Figure 12 shows the temperature and salinity taken around 1630 hours at stations C, M.S., and H stretching across the study area (Fig. 1). In general, the water on the eastern side of the study area was overall slightly saltier below 12 m than that at the weather station and west of it. For comparison the variation over time of the salinity field at the weather station is shown in Fig. 13. Combining the data from Figs. 12 and 13 allows a crude prediction of the induced velocity field in the hypolimnion. There is clearly some evidence that the deep water below 12 m moved east between 1506 hours and 1901 hours, in what appears to be a first-mode response (Monismith 1985). By 1901 hours, the whole water column below 12 m was moving west in more like a combination of first- and second-mode basin

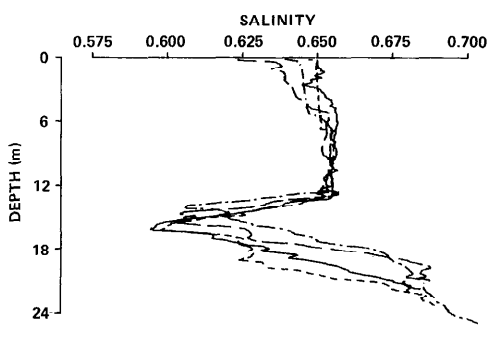


Fig. 13. Salinity (%) as a function of depth at the meteorological station. Solid line—FD 1506; dashed line—FD 1901; broken line—FD 2247; dash-dot line—FD 0428.

response. The deep hypolimnetic water below 14 m continued to move in the same direction until nearly 0428 hours, but it moved eastward above this level. As discussed above, the drogue data suggested an eastward motion in the mixed layer that continued until 1941 hours. After this time the mixed layer moved westward, causing a warming of the surface water at the meteorological station between 1901 and 2247 hours, even though there was a net surface heat loss at the time.

In summary, basin-scale response thus consisted of a strong mixing of the diurnal thermocline down onto the parent thermocline. Once there, the pressure field tilted the parent thermocline quite severely into the water below. The internal heaving deduced from the salinity variations and the drogue motion was consistent with the response of a three-layer system (Monismith 1985). Some evidence was found for an eastward intrusion at the base of the mixed layer between 1901 and 0428 hours. Overall, the return motion of both the mixed layer and the seasonal thermocline was strongly damped. By the morning after the wind event the amplitude of the parent and seasonal thermocline seiches had decreased to <0.3 m at the meteorological station. The damping of the upper-layer motion is consistent with the results of Monismith (1983) at small Wedderburn numbers. However, the observed strong damping of the excited basin-scale sciching remains unexplained.

The details of the mixing process will now be examined. As already seen from Fig. 11, the rate of interface deepening by entrainment was approximately matched by the rate of change of the interface depth due to tilting. This may be expected since W remained below 2 until sometime after 2000 hours. The salinity variation in the lake did not add a significant contribution to the density anomaly, and so the temperature traces shown in Fig. 14 can be examined for any evidence of overturning activity. Overturning signatures were recorded in all CTD casts and most microstructure casts except those taken at 1901 and 2247 hours. Particularly severe instabilities were recorded at 1320, 1631, and 1908 hours.

The vertical extent of an overturning event was calculated by reordering the density profile to make the density increase monotonically with depth. The vertical displacement of any particle required to achieve such a monotonic density profile was first introduced by Thorpe (1977); it characterizes the vertical water particle excursion during an overturning event. All CTD and microstructure data taken during the windy period were processed in this way. The data in a profile were vertically rearranged if the density difference between adjacent particles exceeded 0.002 kg m^{-3} . The resulting vertical displacements were averaged into vertical bins of 0.40 m. The average displacements so computed are shown in Fig. 14b in an overlay plot corresponding to the temperature profiles in Fig. 14a.

Consider first profiles 1320 and 1450; the strong surface events essentially occupied the whole mixed layer, giving a displacement scale of about 0.4–0.5 m in both cases (see Fig. 14b). This indicates that shear production at the base of the mixed layer and the introduction of turbulent kinetic energy near the surface layer formed overlapping regions.

The profile taken at 1506 hours required only minor adjustments to make it monotonic, but by 1620 strong activity was observed around a depth of 2 m. This event was not present in the profile at 1624, taken about 400 m northeast of that at 1620, but internal shear had formed a secondary layer between 2.5 and 4.0 m, with quite sharp boundaries below and above in the temperature profile. At the weather station, a few minutes later, a strong billowing event was recorded in profile 1631, with a displacement scale of about 0.2 m (Fig. 14b). Also noticeable from Fig. 14b is the presence of reasonably strong mixing events around the parent thermocline even before the diurnal thermocline had reached that depth. This would indicate that considerable shear had built up across the parent thermocline, even before the direct influence of the wind was being felt at that depth.

Dillon (1982) showed that for an active overturning event the displacement scale computed as above is representative of the Ozmidov length (see also Imberger and

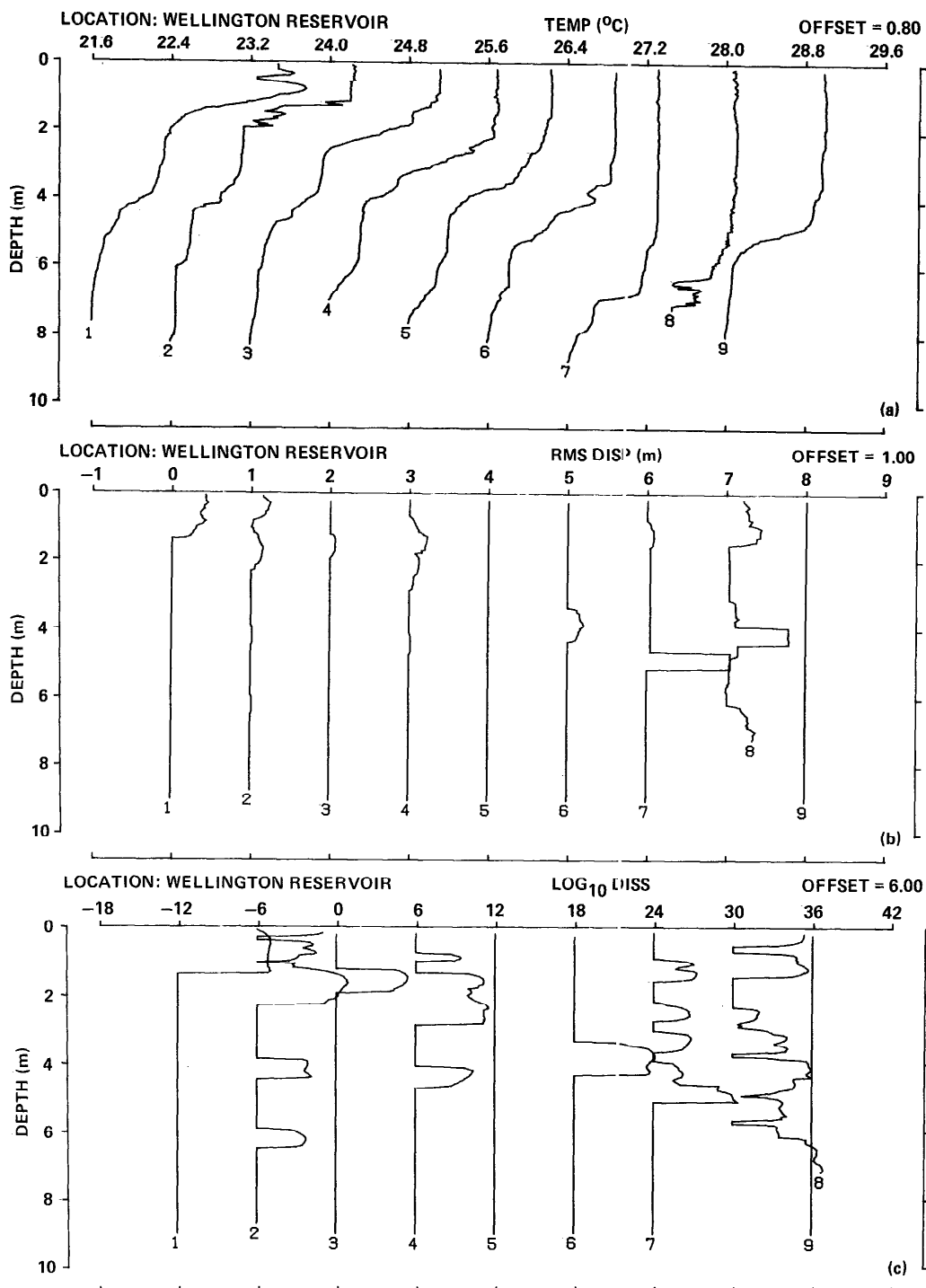


Fig. 14. a. Staggered temperature vs. depth from casts taken throughout the sea breeze period. 1—FD 1320; 2—MT 1450; 3—FD 1506; 4—FD 1620; 5—FD 1624; 6—FD 1631; 7--FD 1901; 8—MT 1908; 9—FD 2247. Note the strong overturning events recorded in profiles 1, 2, 6, and 8. b. Staggered rms displacement l for the profiles shown in Fig. 16a. The bin size for computing the mean was 0.4 m. Large displacements correspond to

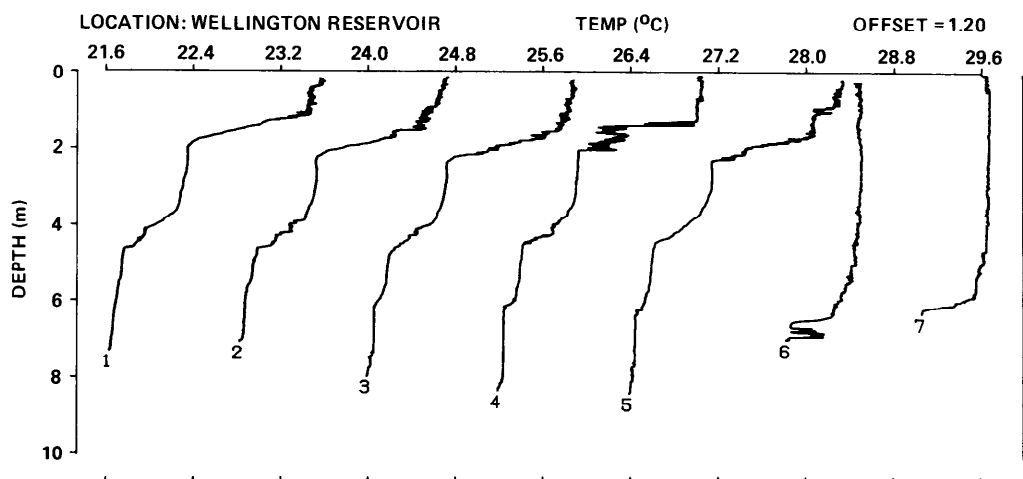


Fig. 15. Staggered temperature vs. depth from the microstructure casts taken throughout the sea breeze period. The mixed layer is seen to be actively turbulent with sporadic overturning events at the base (profiles 4 and 6). 1—MT 1403; 2—MT 1440; 3—MT 1444; 4—MT 1450; 5—MT 1456; 6—MT 1908; 7—MT 1914.

Hamblin 1982). A good estimate of the dissipation of the turbulent kinetic energy may thus be obtained from the quantity $N^3 l^2$, where l is the displacement scale and N the buoyancy frequency, computed from the monotonic density profile and smoothed over the bin size (Fig. 14c). In the strong surface event recorded in profiles 1320 and 1450 and in the event captured at the base of the mixed layer in profile 1908, the dissipation rose to about $10^{-5} \text{ m}^2 \text{ s}^{-3}$, but in most other overturning events the peak dissipation remained $< 10^{-6} \text{ m}^2 \text{ s}^{-3}$.

The dissipation of energy in the water column was also calculated from the 100-Hz temperature gradient time series with the technique developed by Caldwell and Dillon (1981). The spectra computed from these time series were compared to the theoretical predictions of Batchelor (1959) by a non-linear least-squares fit, with the temperature dissipation and the turbulent kinetic energy dissipation as the free parameters. The estimate so obtained depended completely on the very smallest scales of motion near the dissipation cut-off wave number; they are

independent of the previous displacement scale estimates. Further, since the temperature microstructure sensors were able to resolve down to about 1 mm, it was possible to look at the fine grain of the turbulence remaining after the primary collapse of particular overturning events. This provided a measure of the distribution of the actual mixing regions distinct from the sporadic larger events responsible for the major entrainment motions (Corcos and Sherman 1976).

The casts covering the windy period are shown in Fig. 15. The series covers two timespans, first about 1400–1500 hours during which time W was about 0.09, and a second two casts at 1908 and 1914 hours at which W was about 0.86 and the interface was considerably deeper. Further data taken during the same period at stations east and west of the weather station are not shown in Fig. 15 because they were distorted relative to the casts at the weather station due to the tilting of the thermocline. However, all the data were processed to yield spectra and estimates of dissipation as a function

←

active overturning events. The threshold in monotonizing the density was 0.002 kg m^{-3} . c. Staggered estimates of dissipation for the profiles shown in Fig. 16a. The values were obtained from the displacement length l and the buoyancy frequency by forming the product $N^3 l^2$.

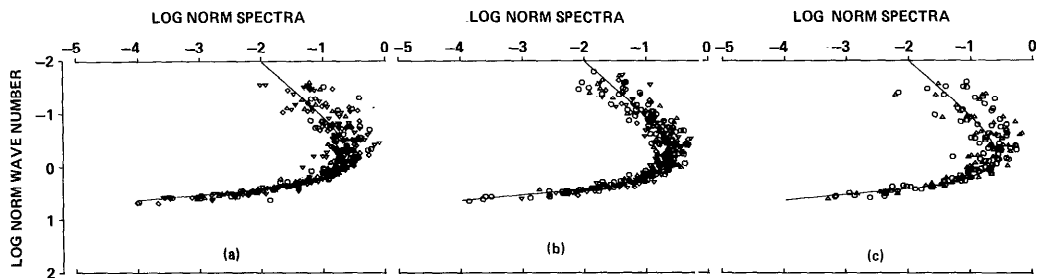


Fig. 16. Normalized temperature gradient spectra: $S(k)k_B D/(q/2)^{\nu} \chi_o$ vs. $k(2q)^{\nu} k_B$ where $S(k)$ is the spectral density ($\text{C}^2 \text{m}^{-2}/\text{CPM}$), k_B is the wave number (CPM), k is the Batchelor wave number ($\epsilon^{-1} D^{-2})^{1/4}$ (CPM), q is a universal constant (3.4), χ_o is the temperature variance dissipation rate ($\text{C}^2 \text{s}^{-1}$) derived from the area under the spectral density times $6D$, D is the molecular diffusivity ($\text{m}^2 \text{s}^{-1}$), ν is the kinematic viscosity ($\text{m}^2 \text{s}^{-1}$), and ϵ is the energy dissipation ($\text{m}^2 \text{s}^{-3}$). Only points with spectra similar to the Batchelor spectra are included. a—Period containing MT 1403, MT 1444, MT 1450, MT 1456; b—period containing MT 1748, MT 1756, MT 1806, MT 1809; c—period containing MT 1908, MT 1914.

of depth. Past practice (see Caldwell et al. 1980) has been to choose only those spectra which very closely fitted the theoretical spectral shape. The best fitting spectra were collected and are plotted nondimensionally in Fig. 16a, b, and c. The fit to the theoretical shape beyond the peak is excellent in all cases, indicating that the underlying assumptions of isotropy and homogeneity are satisfied in these active events. The scatter at the lower wave numbers always arises because the spectra are often contaminated at the low wave number by part of the in-

ternal wave spectral variation (Caldwell et al. 1980). The spectra chosen tended to come from events that were active but had reasonably small displacement scales, because for very severe events the dissipation rose beyond 10^{-5} so that the smaller scales could no longer be resolved with the instrument used. For values $\lesssim 10^{-8}$, noise in the amplification process started to contaminate the spectral data.

Many spectra were also calculated that did not have the exact theoretical spectral shape of a passive tracer, being contami-

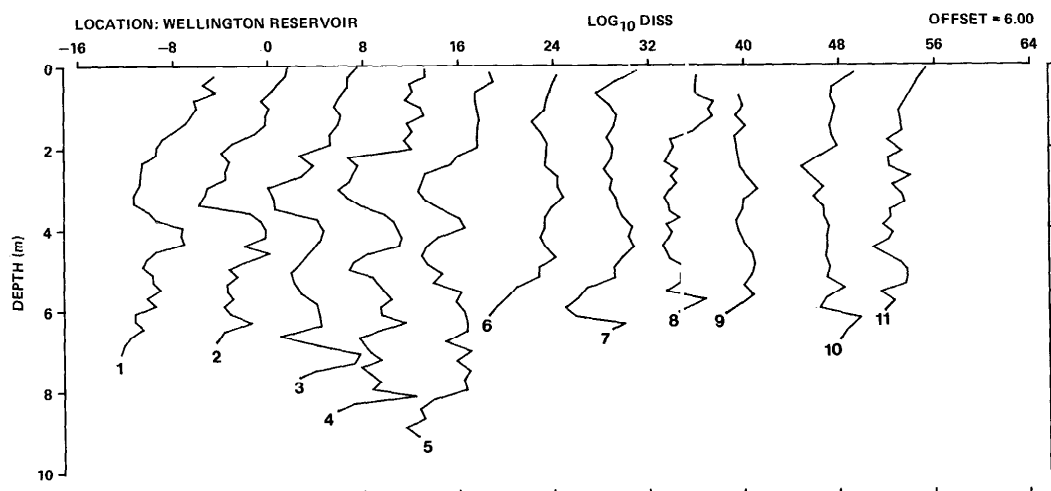


Fig. 17. Raw dissipation estimates from fine-scale casts vs. deptl. for the sea breeze period 1—MT 1403; 2—MT 1440; 3—MT 1444; 4—MT 1450; 5—MT 1456; 6—MT 1748; 7—MT 1756; 8—MT 1806; 9—MT 1809; 10—MT 1908; 11—MT 1914.

nated either by the internal wave subrange or the noise of the instrument. Useful information was gained by analyzing dissipation estimates from partially fitted curves—cases in which the fit mainly relied only on the rising or falling part of the spectral curve. Bad fits and cases where no well defined turbulence spectral shape was observed were excluded. The resulting dissipation estimates are plotted against depth in Fig. 17.

Several consistent trends are discernible from these results. In the surface layer, the dissipation generally decreased with depth; the surface maximum was clearly a function of wind speed, being highest for the casts taken at 1908 and 1914 hours, corresponding to the second windy period (Table 2). The lowest surface values were recorded for casts 1806 and 1809 taken during a lull in the wind. A local maximum is also consistently observed at the parent thermocline depth until profile 1748, at which stage the diurnal thermocline had eroded into the parent thermocline. After this time, the dissipation levels remained reasonably constant throughout the mixed layer, but again, with consistently higher local values at its base. This is in contrast to the earlier casts where there was no local maximum at the base of the mixed layer corresponding to shear production, even though this source of energy was quite large. The large billow size at the time probably smeared the source of energy over most of the very shallow mixed layer.

All the dissipation estimates from the various microstructure casts were collected together in a nondimensional form in Fig. 18. The law-of-the-wall scaling was used since the buoyancy flux had only a minor effect on turbulence at the time. Lumley and Panofsky (1964) and Dillon et al. (1981) showed that a plot of the dimensionless dissipation should have a -1 slope near the surface and pass through the origin. Although the data show a great deal of scatter, the inverse decrease in dissipation is evident over the first 30% of the mixed layer. Below this, the dissipation continued to decrease for the first five profiles, all taken when the mixed-layer depth was <2 m. However, for the later profiles, when the

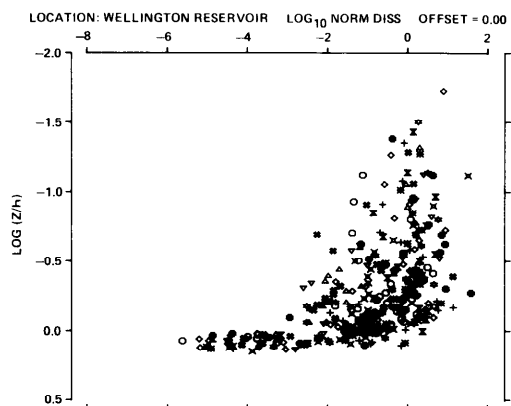


Fig. 18. Nondimensional plot of dissipation vs. depth. All data are included. The dissipation was dimensionalized with the buoyancy flux B (Table 2) and the depth with h .

mixed layer had deepened to well over 4 m, Fig. 18 shows that the dissipation rose considerably just above the base of the mixed layer. This is particularly noticeable for the dissipation estimates derived from profile 1908 (\diamond : Fig. 18) which captured the very large overturning event just above the thermocline (see Fig. 15). The very large scatter in the bottom half of the profile suggests sporadic overturning events and very patchy turbulence consistent with billowing at the base of the mixed layer. Below the mixed layer the nondimensional dissipation decreased quite rapidly down to 10^{-6} . The increase at $\log_{10}(z/h)$, equal to 0.6, was mainly due to the turbulence occurring in the early profiles at the 4-m interface (see Figs. 14c and 17).

In summary, the afternoon data allowed documentation of the development of a diurnal mixed layer which deepened into the parent diurnal thermocline. The value of W was small throughout the afternoon; large-scale billow events were observed from the very beginning of the windy period. Shear associated with both the first and second internal modes of the density profile built up rapidly, causing the thermocline to tilt at a rate comparable to the deepening due to entrainment. At the beginning of the period, the mixed layer was extremely shallow; it remained so due to the strong solar radiation of the early afternoon. This led to

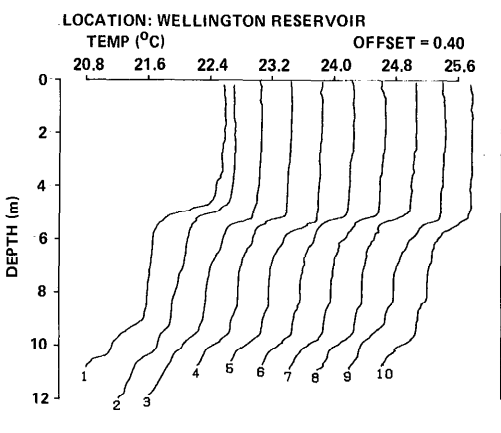


Fig. 19. Staggered fine-scale temperatures vs. depth for the convective period. 1—FD 2247; 2—FD 0330; 3—FD 0428; 4—FD 0445; 5—FD 0447; 6—FD 0449; 7—FD 0450; 8—FD 0451; 9—FD 0510; 10—FD 0627.

billows that were of the same size as the mixed layer; consequently, the turbulent kinetic energy source from both shear production and that introduced at the surface was smeared over the whole mixed layer. By contrast, by the time the layer had deepened to about 5 m, a very distinct separation had occurred between the surface introduction of turbulence and the internal generation by shear production at the base of the mixed layer. The dissipation appeared to follow simple, neutral boundary-layer scaling in the top 30% of the mixed layer, but a great deal of scatter at the base of the mixed layer was documented, indicating that the source of turbulence in this region was of a larger scale and very much more sporadic. Lastly, momentum was transmitted to the parent diurnal thermocline and well below before the wind mixing had penetrated to that level. The shear across the parent thermocline was sufficient to induce quite a large dissipation in the thermocline.

Convective cooling—Period 3

The sea breeze activity continued into the late evening, but by 2300 hours the wind had dropped to $<1.0 \text{ m s}^{-1}$ (see Fig. 3d). The rest of the night and the following early morning were characterized by calm conditions, with only a very weak breeze gently moving the air across the glassy water surface. The air temperature dropped to $<10^\circ\text{C}$,

causing a temperature differential across the air-water interface of $>12^\circ\text{C}$. During the early morning, the net heat flux out of the water surface was reasonably steady, and the value of $|l/h|$ (see Table 2) was extremely small so that the deepening of the mixed layer was completely dominated by natural convective processes from 2247 hours onward.

Under such circumstances, Eq. 9 can be simplified:

$$\frac{R}{R_0} = f\left(\frac{z}{h}\right) \quad (15)$$

where the Peclet number is assumed to be very large (and nearly constant) and thus no longer influences the entrainment (Denton and Wood 1981). Near the water surface free convection processes prevailed, making any expression, such as Eq. 15, independent of the mixed-layer depth h . This means that any property R of the fluid motion can only depend on the surface buoyancy flux B and possibly the depth z , both of which must enter Eq. 15 through the parameter R_0 .

With this in mind, consider the period from 2247 to 0629 hours. After the tow out of Study Creek at 2315 hours (see above), mechanical problems interfered until 0330. A series of CTD casts was then initiated at the meteorological station, and these were continued through to daybreak at 0629 hours. Interspersed between the CTD casts were a set of 11 casts with the rising microstructure vehicle; my discussion here is confined to the dissipation of turbulent kinetic energy and its relationship to the predictions from the numerical simulation discussed later.

The temperature-time variation from the CTD casts is shown in Fig. 8. The slight warming around 2247 hours marked the end of the recovery from the wind-induced tilt. After the cast at 0330 hours, the mixed-layer temperature decreased again (see Figs. 8 and 19), but the deepening process had slowed considerably. Also noticeable is the distinct shoulder at 3.74 m in the profile taken at 2247 hours (Fig. 19), indicating a recession in the mixed-layer depth due to thickening of the interface by active billowing during the active shear period. Natural

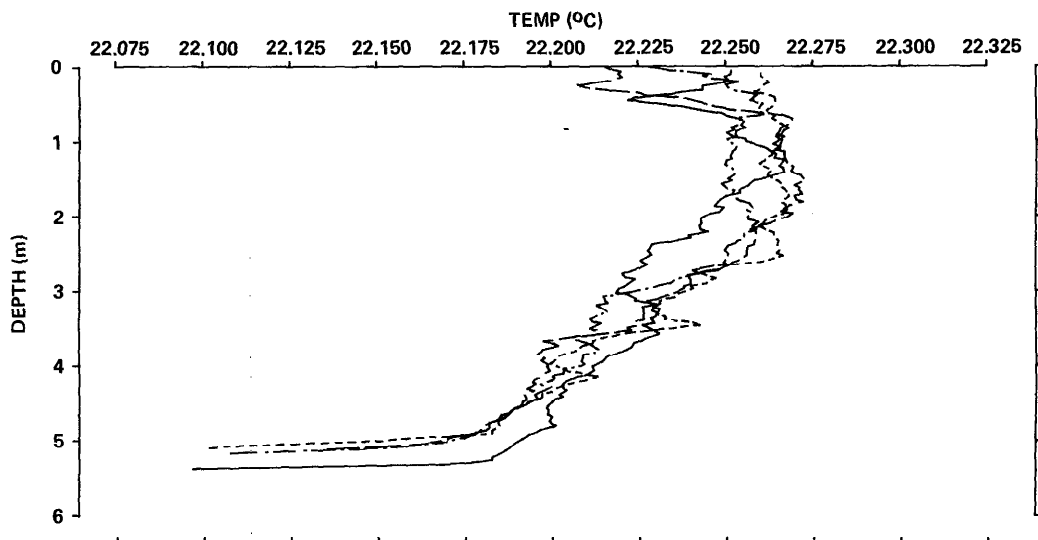


Fig. 20. Expanded fine-scale temperature profiles for the convective period showing unstable region near the surface. Solid line—FD 0447; dash-dot line—FD 0449; broken line—FD 0450; dashed line—FD 0451.

convection had eroded most of this by 0330 hours. Evidence of very weak seiching remained throughout the night; the base of the mixed layer and the seasonal thermocline moved vertically by about 0.3 m.

The temperature profiles in the mixed layer show a distinct concave trend, with temperatures at the surface and at the base of the mixed layer being somewhat lower than those in the central region of the mixed

layer itself (Fig. 20). The temperature maximum occurred at about 1.8 m, and the layer depth was about 5.4 m. Thus while the upper 30% of the mixed layer was undergoing free natural convection, the rest of the surface layer was quite strongly influenced by the stable stratification at the base of the mixed layer.

The microstructure traces are shown in an offset plot in Fig. 21. Particularly no-

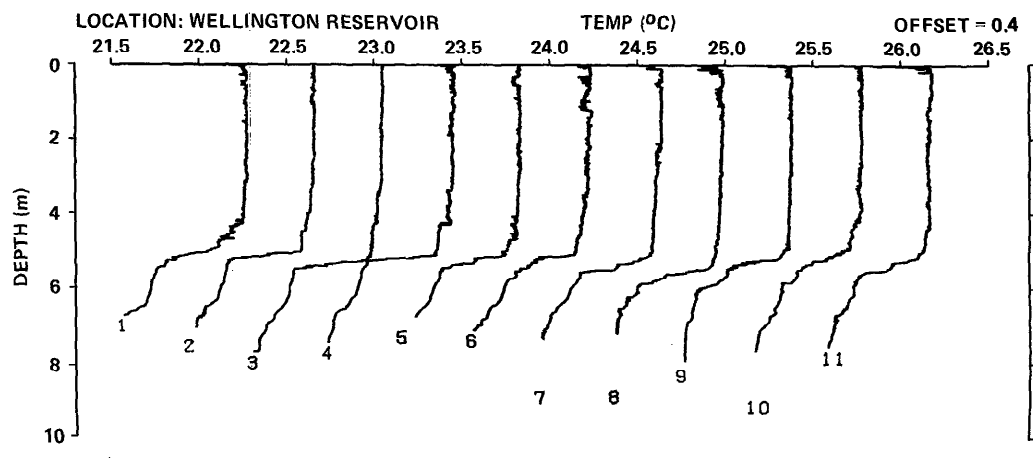


Fig. 21. Staggered microstructure temperature profiles for the convective period. Profiles clearly show the formation and propagation of thermals at the surface. 1—MT 0409; 2—MT 0413; 3—MT 0419; 4—MT 0423; 5—MT 0455; 6—MT 0459; 7—MT 0504; 8—MT 0609; 9—MT 0613; 10—MT 0617; 11—MT 0621.

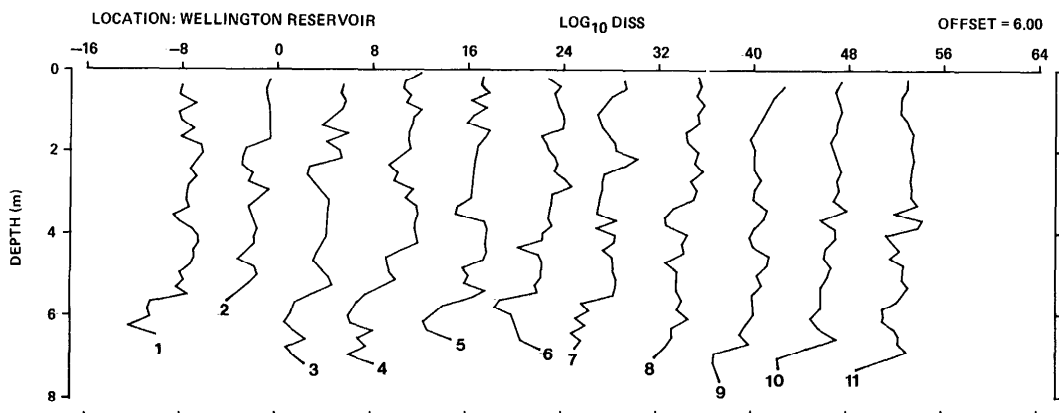


Fig. 22. Raw dissipation estimates from fine-scale casts vs. depth for the convective period. Profile numbers same as Fig. 21.

ticeable is the varied nature of the temperature fluctuations. On some casts (0413, 0613, 0617) the temperature was almost constant immediately beneath the free surface, yet in others (0409, 0423, 0609, 0621) a distinctly unstable layer had formed beneath the surface, suggesting the formation of falling thermals. The trace taken at 0459 hours shows evidence, at about 1 m, of such a temperature deficit. Also noteworthy is the variability recorded in the details of the shape of the base of the mixed layer; in some instances there was a very sharp interface, in others the interface was quite broad.

The dissipation in the mixed layer was again calculated with the spectral fitting package in order to determine the mean dissipation within the mixed layer, as well as the position of maximum dissipation, and so the most likely level of production of turbulent kinetic energy (Fig. 22). Distinct from the earlier wind-driven period (Fig. 17), the dissipation in the mixed layer showed no observable trends with depth but fluctuated around a constant value over most of the mixed-layer depth. Below, in the strong temperature gradient region, the dissipation decreased rapidly by nearly a factor of 10^3 .

Dimensional reasoning (Kaimal et al. 1976) suggests that $\epsilon \sim B$. All the dissipation data from Fig. 22 were collected on a dimensionless plot in Fig. 23. There is again considerable scatter in the measurements, with some indication of higher values near

the surface. The depth-averaged value of the dissipation from all the data in the mixed layer, $-0.45B$, is in excellent agreement with that measured by Shay and Gregg (1984) in the ocean and in good agreement with measurements taken in the atmospheric boundary layer by Kaimal et al. (1976), Willis and Deardorff (1974), Mahrt and Lenschow (1976), and Guillemet et al. (1983) who all found that the dissipation ranged between 0.30 and $0.80B$.

The vertical heat flux, calculated from the time rate of change of the temperature of the water column for three periods during the convective phase, was upward toward the water surface over the whole mixed-layer depth (Fig. 24). This is similar to what was found by Kaimal et al. (1976) in the atmospheric boundary layer. The consequence of this variation, when combined with the shape of the mean temperature gradient (Fig. 20), is that the heat was moved with the mean gradient only in the free convecting zone, but against the mean temperature gradient in the bulk of the mixed layer. It is clear that the temperature fluctuations can only survive in the bulk of the mixed layer if these fluctuations are constantly revitalized from the free convecting zone where they are created. Counter-gradient transport such as observed here is commonly encountered in atmospheric measurements (see discussion by Therry and Lacarrère 1983).

In summary, the early morning period of

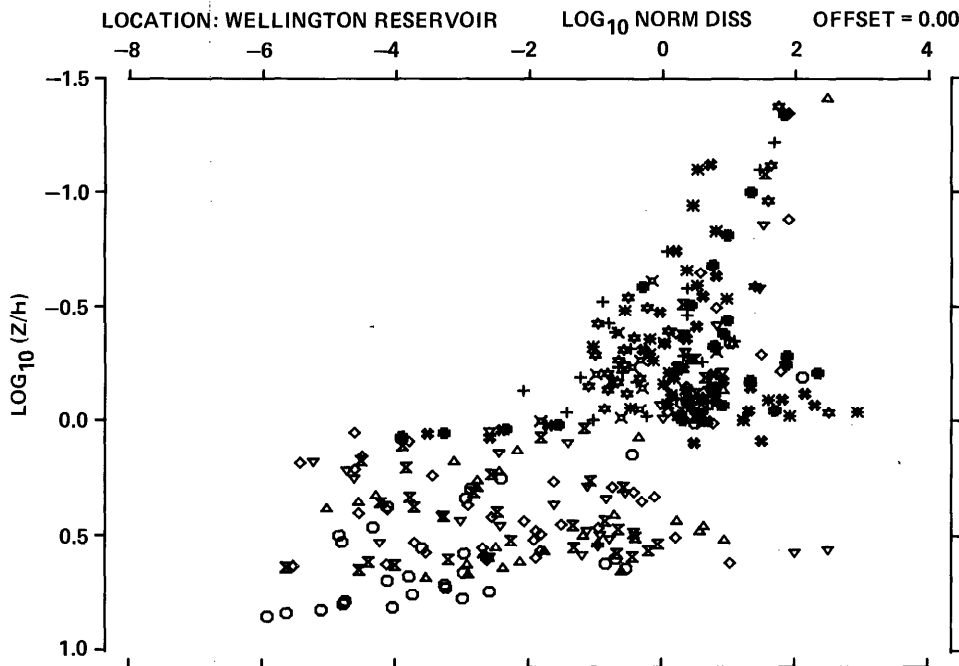


Fig. 23. Normalized dissipation vs. normalized depth for the sea breeze period. Dissipation was dimensionalized with u_*^3/kh , where k is the von Karman constant ($=0.4$) and depth was dimensionalized with h . All spectral estimates were included.

14 March presented ideal conditions for measuring the properties of a strongly convecting mixed layer. The rate of entrainment was considerably less than that due to shear production observed in the windy period. However, unlike mechanical mixing, natural convection reduced the temperature difference across the base of the mixed layer and thus decreased the thermocline stability, making it more susceptible to future wind-driven entrainment.

Application of an integral model

The field data showed that the behavior of the diurnal mixed layer on 13 and 14 March could be conveniently partitioned into reasonably discrete periods. First, there was the morning heating period, when the whole upper water column was heated and thus stabilized, but the base of the mixed layer was actually strongly billowing. Second, during the period of intense wind, the layer deepened by the combination of surface-introduced turbulence, internal shear production, penetrative convection, and

upwelling. The wind quickly spun up the turbulence field and deepened the layer a little beyond the parent mixed-layer depth remaining from the previous evening. Third, the net loss of heat from the surface at night caused the mixed layer to cool, thus weakening the density jump at the base. The weakened mixed-layer base then became increasingly susceptible to the mechanical energy derived from the buoyancy flux during this period.

The behavior of such diurnal mixed layers in the atmosphere has been modeled by various techniques (Deardorff 1974). Driessens (1982) has shown that even the simplest models give satisfactory predictions under a wide variety of conditions. It is, however, instructive to investigate the turbulent kinetic energy budget in the mixed layer during the different periods of deepening. This may be done conveniently with a recently constructed simple integral model of the mixed layer. The aim was to see whether the simple unsteady terms in the turbulent kinetic energy are an appreciable

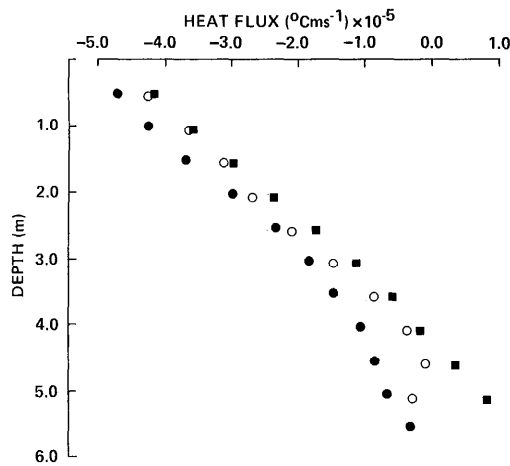


Fig. 24. Heat transfer ($w'\theta'$) calculated from changes in heat content of the water column. Period from 0510 to 0627 hours using FD files 0510 and 0627—●; period from 0415 to 0500 hours using average of MT files 0409, 0413, 0419, 0423 and 0455, 0459, 0504—○; period from 0500 to 0615 hours using average of MT files 0455, 0459, 0504 and 0609, 0613, 0617, 0621—■.

percentage of the total kinetic energy during periods of rapid deepening. The model also helped separate the changes in the mixed-layer behavior due to vertical mixing processes from those induced by horizontal advection.

The model used is an adaptation of the algorithm developed by Rayner (1980), different mainly in the formulation of the momentum calculation. I used Eq. 10 over a specified time interval, starting the integration at the beginning of the simulation and stopping it at a time corresponding to the maximum shear velocity. After this, the mixed-layer velocity was allowed to decay linearly over a specified decay time. The start, stop, and decay times were not calculated but determined from examination of the data in Fig. 8. The parameterization of the turbulent kinetic energy equation in the model was patterned on the original work of Niiler (1975), Zilitinkevich (1975), and Zeman and Tennekes (1977). A full description of such models is given by Kraus (1977) and Fischer et al. (1979). The main feature of the model is that the input of turbulent kinetic energy at the surface of the lake is used first to initiate a turbulent kinetic en-

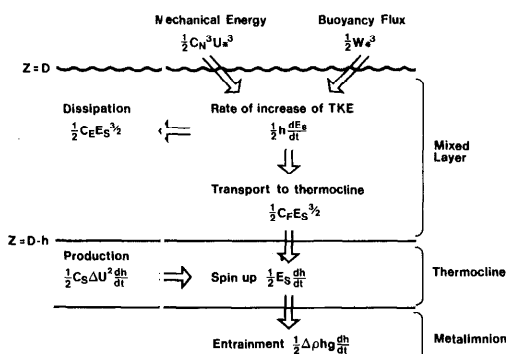


Fig. 25. Schematic of the turbulent energy flux paths assumed in model.

ergy field in the mixed layer; only after the field becomes established is this energy brought to bear on the base of the mixed layer. In this way, the turbulent kinetic energy store in the mixed layer provides an important buffer between the rate of working of the wind (and also the rate of introduction of potential energy by any negative buoyancy flux) and the rate of working at the base of the mixed layer by the turbulence. Such a model thus allows examination of energy partitioning during periods of rapidly changing inputs.

A formal integration of the turbulent kinetic energy equation (Rayner 1980; Kraus 1977) leads to a balance of energy as indicated in Fig. 25. The mechanical energy introduced at the water surface is derived from the work done by pressure fluctuations, the shear production in the wind surface shear layer, and from the availability of mechanical energy derived from surface cooling. Kim (1976) and Fischer et al. (1979) showed that the energy flux F_q derived from these three sources can be parameterized by

$$F_q = \frac{q_*^3}{2} = \frac{1}{2}(w_*^3 + C_N^3 u_*^3) \quad (16)$$

where w_* is defined in Eq. 5 and C_N is a constant.

Deepening at the base of the mixed layer leads to a release of mean kinetic energy, which is converted to a turbulent kinetic energy source by the Reynolds stress terms.

Niiler (1975) showed that this shear production flux F_s can be parameterized as

$$F_s = \frac{C_S}{2} \Delta U^2 \frac{dh}{dt} \quad (17)$$

where C_S is a constant, ΔU is the velocity jump across the base of the mixed layer, and dh/dt is the rate of deepening of the mixed layer. At this stage both the change of kinetic energy and potential energy associated with billowing should be included in the energy budget (see Imberger and Patterson 1980); this improves the fit near the base of the mixed layer of the predicted profiles. However, since the main purpose of this investigation was to verify the temporal resolution, the introduction of the billowing mechanism was unnecessary here. The dissipation flux F_d in the mixed layer is assumed to depend on the kinetic energy (Mahrt and Lenschow 1976) so that

$$F_d = -\frac{C_E}{2} E_s^{3/2} \quad (18)$$

where $\frac{1}{2}E_s$ is the average kinetic energy per unit mass in the mixed layer.

Entrainment is assumed to cause a change of potential energy of the mixed layer as a whole and the potential energy flux F_p is given by

$$\begin{aligned} F_p &= \frac{1}{2} \frac{\Delta \rho h g}{\rho} \frac{dh}{dt} \\ &= -\frac{1}{2} (\alpha g \Delta T - \beta g \Delta S) g h \frac{dh}{dt} \end{aligned} \quad (19)$$

where ΔT and ΔS are the temperature and salinity jumps at the base of the mixed layer, assumed to be positive for a stable density change. The constant α is the coefficient of expansion and β is the coefficient of density change for unit salinity change.

In the mixed layer, the rate of change of kinetic energy in the water column is given by

$$\frac{d}{dt} \left(\frac{1}{2} h E_s \right) = \frac{h}{2} \frac{dE_s}{dt} + \frac{E_s}{2} \frac{dh}{dt}. \quad (20)$$

Rayner (1980) assumed separate energy balances in the mixed layer and the base of the mixed layer. In the mixed layer, the tur-

bulent kinetic energy balance was assumed to be

$$\begin{aligned} \frac{h}{2} \frac{d}{dt} E_s &= \frac{q_*^3}{2} - \frac{C_E}{2} E_s^{3/2} \\ &\quad - \frac{C_F}{2} E_s^{3/2} \end{aligned} \quad (21)$$

where the internal rate of working F_i of the turbulence on the interface was parameterized (Zeman and Tennekes 1977):

$$F_i = -\frac{C_F}{2} E_s^{3/2} \quad (22)$$

and C_F is a constant. The energy balance at the base of the mixed layer is thus simply a balance of gains and losses:

$$\begin{aligned} \frac{C_F}{2} E_s^{3/2} + \frac{C_S}{2} \Delta U^2 \frac{dh}{dt} \\ = \frac{1}{2} \Delta \rho h g \frac{dh}{dt} + \frac{E_s}{2} \frac{dh}{dt}. \end{aligned} \quad (23)$$

Equations 21 and 23 together with the thermal budget in the mixed layer and the appropriate boundary conditions form a closed system of equations for E_s and h , with four constants C_N , C_S , C_E and C_F . The values of these coefficients can be determined from experimental results. Rayner (1980) gave a good summary of available experimental information and recommended the values

$$C_N = 1.33, \quad C_S = 0.20, \quad C_E = 1.15, \quad \text{and} \quad C_F = 0.25. \quad (24)$$

Before discussing the simulations using these values, I will compare the efficiency of energy conversion that follows from the coefficient values with those predicted from the present field measurements. This is most easily done under equilibrium conditions, where

$$q_*^3 = (C_E + C_F) E_s^{3/2}. \quad (25)$$

The dissipation ratio,

$$\frac{\text{Rate of energy dissipation}}{\text{Surface energy flux}} = \frac{C_E E_s^{3/2}}{q_*^3}, \quad (26)$$

under equilibrium conditions has the model value of $C_E : (C_E + C_F)$ which is equal to

0.82 with the values in Eq. 24. Stable conditions existed during period 3 when natural convection processes dominated the behavior of the mixed layer and the surface fluxes were nearly constant. As discussed above, the ratio $\epsilon:B$ was 0.45, which means that the dissipation ratio $2\epsilon h:w_*^3$ was equal to 0.9, in good agreement with previous work in the atmospheric boundary layer and with the value used in the model simulation.

The efficiency C_s of the shear production source is more difficult to verify since the energy introduced by production at the base of the mixed layer is immediately utilized to entrain fluid from beneath, and much of it is also directly dissipated. However, an approximate estimate follows if Eq. 21 and 23 are rewritten assuming the turbulence is in equilibrium and the temporal entrainment terms are small:

$$C_s = \frac{g'h}{\Delta U^2} - \frac{q_*^3}{\frac{dh}{dt}\Delta U^2} \left\{ 1 - \frac{2\epsilon h}{q_*^3} \right\}. \quad (27)$$

The last term is just the ratio of the dissipation to the surface inputs, assumed to be equal to 0.82, so that

$$C_s = \frac{g'h}{\Delta U^2} - \frac{0.18 q_*^3}{\Delta U^2 \frac{dh}{dt}}. \quad (28)$$

The difficulty with evaluating this estimate is that the rate of change of depth was strongly influenced by tilting of the interface, and any estimate of C_s must be made before tilt influenced the deepening. The time period around 1500 hours should be satisfactory, as the internal interfacial wave had not arrived at this site as yet. From Table 2, $h = 1.7$ m, $g' = 2.5 \times 10^{-3}$ m s $^{-2}$, $q_*^3 = 5.43 \times 10^{-7}$ m 3 s $^{-3}$ and $dh/dt = 0.8/6,000 = 1.33 \times 10^{-4}$. The shear ΔU can be estimated from Eq. 13 as 0.116 m s $^{-1}$. Substituting these values into Eq. 28 leads to a value for C_s of 0.24, in very good agreement with the value given in Eq. 24.

To compare the complete dynamical behavior of the model with the observed results, I ran the simulation from 1017 hours on 13 March to 0630 hours on 14 March.

The only remaining unknown parameters are the solar extinction coefficients (Table 2). Unfortunately, no data existed for their evaluation. Previous data (Rayner 1980) were used to determine the coefficients A_3 and β_3 and the rest chosen to yield the correct peak temperature at 1200 hours on 13 March. The choice of these constants did not greatly influence the mixed-layer depth, since gain in potential energy due to H_* was small at all times.

As discussed above, tilting of the interface led to a subsequent rebounding of the isotherms with an associated increase in temperature in the mixed layer between 1941 and 2247 hours. The active billowing during the period of strong shear left a much smoothed profile at 2247 hours with a mixed layer restarting at 3.74-m depth (Fig. 14a, profile 9). Neither advection nor smearing of the profile can be reproduced with the present model.

The mixed-layer temperature is reproduced extremely well except for the period between about 1700 and 1941 hours, where the field data show a somewhat more rapid rate of cooling than the model results (Fig. 26j). There was a definite temperature gradient in the mixed layer across the study zone during this period; an approximate estimate of it is 2.5×10^{-4} °C m $^{-1}$ (Fig. 9). Since the average mixed-layer velocity at the time was 0.1 m s $^{-1}$, the advection of this gradient would have led to a further temperature decrease of about 0.24°C in 3 h, in very close agreement with the observed mismatch.

The simulated mixed-layer depth and the measured data (Fig. 26g) agree well until about 1700 hours, at which time the thermocline tilting induced an apparent deepening at the weather station. The buildup of the horizontal temperature gradient in the mixed layer thus corresponded quite well to onset of the thermocline tilt. The rebound accounted for most of the tilt-induced deepening, but after the seiching had subsided the mixed-layer depth was a little shallower (0.6 m) than that simulated and the actual mixed-layer temperature was slightly warmer (0.1°C) than that simulated. These discrepancies indicate the need to capture smearing of the interface by billowing and

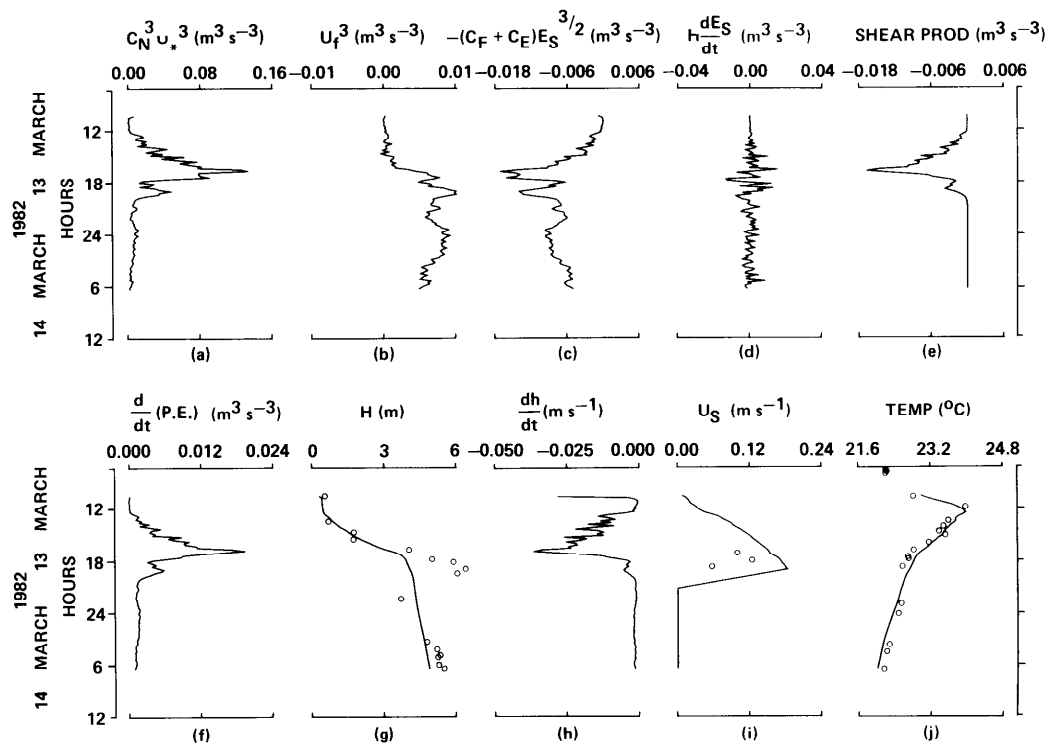


Fig. 26. Model output and comparison with field data. a—Stirring energy flux times two; b—buoyancy energy flux times two w_*^3 ($=3$); c—energy flux lost to dissipation and entrainment at the base times two; d—rate of increase of turbulent kinetic energy in mixed layer times two; e—shear production energy flux times two; f—rate of change of potential energy times two; g—mixed-layer depth (solid line) and experimental values (\circ) from Table 2; h—rate of change of mixed-layer depth; i—mixed-layer average speed (solid line) and drogue measurements (\circ); j—average mixed-layer temperature (solid line) and experimental values from CTD casts (\circ).

the formation of horizontal gradients induced by upwelling.

The velocity computation involved integration of Eq. 10. The time of peak velocity was set at 1900 hours, three-quarters of an hour before the structure had achieved its maximum tilt and the decay time was assumed to be 2 h (Fig. 8). The computed velocities and the drogue velocity data are shown in Fig. 26i. It appears that the computed velocity was about 20% higher than that measured experimentally and that the decay was a little slower than the field measurements. Combined, these two factors would lead to a slight overestimation of the shear production during the late stage of the wind event. However, since the model did not explicitly take into account interfacial billowing, boundary mixing, and mixing due to upwelling, I resisted the temptation of empirically adjusting any of the parameters.

The energy budgets are shown in Fig. 26a–d, with the factor two removed for ease of presentation. The energy dissipation ($C_E/2 \times E_S^{3/2}$) and the export to the base of the mixed layer ($\frac{1}{2}C_F E_S^{3/2}$) are shown in Fig. 26c as a negative quantity. The left-hand side of Eq. 21, the spin-up of the turbulent kinetic energy, is shown in Fig. 26d. It is clear that during the buildup of the wind (up to 1648 hours), the spin-up of turbulent kinetic energy was a considerable drain on the energy budget. The rate of increase of turbulent kinetic energy accounted for nearly 15% of the energy input from q_*^3 . This turbulent kinetic energy was then available for further entrainment after the wind had started to decrease. The unsteady term thus represents a significant store of energy in the overall energy budget of the mixed-layer dynamics.

Shear production naturally depended directly on the shear across the mixed-layer

base. Thus the energy source shown in Fig. 26e follows naturally from the shear production shown in Fig. 26i. Comparison of Fig. 26a and b with 26e, shows that q_{*}^3 was about equal to the shear production during period 2, but much of the surface input was dissipated in the mixed layer itself. Comparison of the rate of exchange of potential energy and shear production shows that the balance in Eq. 23 was predominantly between these two terms; the turbulent diffusion term $C_F/2 \times E_S^{3/2}$ and the entrainment term $E_S/2 \times dh/dt$ were both quite small. Thus the model illustrates the conjecture of Pollard et al. (1973) that a simple Froude number criterion, as given by Eq. 11, suffices as a first estimate of the mixed-layer deepening process.

Conclusions

Fine-scale measurements and microstructure data were used to describe the diurnal behavior of a mixed layer in the Wellington Reservoir in Western Australia. The data covered a morning period of solar heating, a period of severe wind mixing induced by an afternoon sea breeze, and a period of pure penetrative convection extending throughout the night.

Analysis of the data revealed the buildup, in the morning, of a strong surface thermal gradient with very low Wedderburn numbers. This condition led to active billowing even though the layer was heating at the time and the wind speed was low. As the wind increased at the beginning of the sea breeze period the Wedderburn number remained <1 , even though the mixed layer deepened appreciably. The mixed layer responded by tilting in the direction of the wind, causing upwelling at the upwind boundary leading to the formation of horizontal density gradients in the mixed layer itself. The degree of tilt of the mixed-layer base and the damped return to the neutral horizontal state at the cessation of the wind agreed with the predictions of Spigel and Imberger (1980) and the experimental results of Monismith (1983). However, the field data showed less evidence of seiching of the hypolimnion water than predicted by Monismith (1985). The actual deepening of the base of the mixed layer over the total

sea breeze period was less than could be explained with a single slab, one-dimensional mixed-layer model; the decrease was ascribed to active billowing smearing out the strong gradient region. Little direct evidence was recorded of the presence of intrusions resulting from this upwelling. However, it did seem that a disturbance was set up at the cessation of the wind resembling a weak intrusion at the base of the mixed layer. The mixing associated with the upwelling itself was just upwind of the study area and so the broadening of the thermocline observed by Monismith (1983) could not be verified.

The mixed-layer model developed by Rayner (1980) proved most satisfactory and the suggested efficiencies were verified. Overall nearly 82% of the surface energy was lost to dissipation in the mixed layer at any particular time, the remainder being used to deepen the layer. The shear production coefficient was also verified and a value of 0.2 is recommended. The energy balance derived from the model clearly showed that the details of the deepening process depended critically on all the terms in the equation with a rate of increase of turbulent kinetic energy accounting for up to 15% of the surface energy input. However, it was demonstrated that the overall average daily depth of the mixed layer could be predicted satisfactorily by adopting the Pollard et al. (1973) criterion where only shear production is utilized. The question posed in the introduction thus depends critically on the time step of the mixed-layer simulation. For diurnal simulations, all terms plus upwelling must be included; for seasonal simulations a simple Froude number criterion would most likely suffice.

The investigation of turbulent structure showed some interesting results. Evidence was gathered for the existence of a law-of-the-wall layer very near the surface during the period of the developing wind. However, more detailed measurements and more constant wind conditions would be required to improve the verification. Shear production was consistently observed whenever W was <2 and the wind was increasing, with the billows concentrated around the base of the mixed layer once the mixed layer was

greater than the billow height. The production was sporadic and involved overturn length scales of the order of 0.20 m distributed in a very patchy fashion. Estimates of dissipation from temperature microstructure showed a more even distribution, but yielded about the same peak values. However, the spectral shapes deteriorated very quickly immediately after the collapse of strong overturning events. The conclusion to be drawn from this is that once the shear had built up, relatively large billows formed which then collapsed vertically leading to a more even distribution of smaller fossil structures (Gibson 1980). Once the wind had subsided a considerably smoothed profile remained, which was seen to be eroded anew by the convective cooling.

Dissipation estimates in the mixed layer during the penetrative convection period agreed with predictions from equilibrium theory but showed somewhat larger scatter than is normally observed in the atmospheric boundary layer.

The overall conclusions from this study are that the classification scheme for mixed-layer dynamics based on the magnitude of the Wedderburn number appears to be satisfactory, but the assumption of one-dimensionality breaks down once the Wedderburn number is $\lesssim 2$. For such severe wind conditions, upwelling leads to the formation of horizontal gradients and these must be accounted for in the entrainment process at the base of the mixed layer. Further, I suggest that the damping of seiching of the hypolimnion structure was influenced by mixed-layer dynamics for small values of W . The details of the interaction between the mixed-layer tilt and other internal wave basin scale modes need further explanation.

References

- BATCHELOR, G. K. 1959. Small scale variations of convected quantities like temperatures in a turbulent field. *J. Fluid Mech.* **5**: 113–133.
- BLANTON, J. O. 1973. Vertical entrainment into the epilimnia of stratified lakes. *Limnol. Oceanogr.* **18**: 697–704.
- CALDWELL, D. R., AND T. M. DILLON. 1981. An oceanic microstructure measuring system. Oregon State Univ. School Oceanogr. Tech. Rep. Ref. 81-10.
- , —, J. M. BRUBAKER, P. H. NEWBERGER, AND C. H. PAULSON. 1980. The scaling of vertical temperature gradient spectra. *J. Geophys. Res.* **85**: 1917–1924.
- CHURCH, J. A., AND R. O. THOMPSON. 1982. Cloud in cell and finite difference model for a stratified lake, p. 445–469. In J. Noye [ed.], *Numerical solutions of partial differential equations*. North-Holland.
- CORCOS, G. M., AND F. S. SHERMAN. 1976. Vorticity concentrations and the dynamics of unstable shear layers. *J. Fluid Mech.* **73**: 241–264.
- CSANADY, G. T. 1972. Response of large stratified lakes to wind. *J. Phys. Oceanogr.* **2**: 3–13.
- DEARDOFF, J. W. 1970. Convective velocity and temperature scales for unstable planetary boundary layer and for Rayleigh convection. *J. Atmos. Sci.* **27**: 1211–1213.
- . 1974. Three-dimensional numerical study of turbulence in an entraining mixed layer. *Boundary-Layer Meteorol.* **7**: 199–226.
- DENTON, K. A., AND I. WOOD. 1981. Penetrative convection at low Peclet number. *J. Fluid Mech.* **133**: 1–21.
- DILLON, T. M. 1982. The mixing length of vertical overturns: A comparison of Thorpe and Ozmidov length scales. *J. Geophys. Res.* **87**: 9601–9613.
- , J. G. RICHMAN, C. G. HANSEN, AND M. D. PEARSON. 1981. Near-surface turbulence measurements in a lake. *Nature* **290**: 390–392.
- DRIEDONKS, A. G. 1982. Models and observations of the growth of the atmospheric boundary layer. *Boundary-Layer Meteorol.* **23**: 283–306.
- FISCHER, H. B., E. J. LIST, R. C. KOH, J. IMBERGER, AND N. H. BROOKS. 1979. Mixing in inland and coastal waters. Academic.
- GIBSON, C. H. 1980. Fossil temperature, salinity and vorticity turbulent in the ocean, p. 221–257. In J. C. Nihoul [ed.], *Marine turbulence*. Elsevier.
- GUILLEMET, B., H. ISAKA, AND P. MASCART. 1983. Molecular dissipation of turbulent fluctuations in the convective mixed layer. Part 1. Height variations of dissipation rates. *Boundary-Layer Meteorol.* **27**: 141–162.
- HEAPS, N. S., AND A. E. RAMSBOTTOM. 1966. Wind effects on water in a narrow two-layered lake. *Phil. Trans. R. Soc. Lond. Ser. A* **259**: 391–430.
- HICKS, B. B. 1975. A procedure for the formulation of bulk transfer coefficients over water. *Boundary-Layer Meteorol.* **8**: 515–524.
- IMBERGER, J., AND P. F. HAMBLIN. 1982. Dynamics of lakes, reservoirs, and cooling ponds. *Annu. Rev. Fluid Mech.* **14**: 153–187.
- , AND J. C. PATTERSON. 1980. A dynamic reservoir simulation model-DYRESM-5, p. 310–361. In H. B. Fischer [ed.], *Transport models for inland and coastal waters*. Academic.
- KAIMAL, J. C., AND OTHERS. 1976. Turbulence structure in the convective boundary layer. *J. Atmos. Sci.* **33**: 2152–2169.
- KEULEGAN, G., AND V. BRAME. 1960. Fourteenth progress report on model laws for density currents: Mixing effects of wind-induced waves. *Natl. Bur. Std. Rep. NBS-6638*, 35 p.
- KIM, J.-W. 1976. A generalized bulk model of the oceanic mixed layer. *J. Phys. Oceanogr.* **6**: 686–695.

- KRAUS, E. B., ED. 1977. Modelling and prediction of the upper layers of the ocean. Pergamon.
- LUMLEY, J. L., AND H. A. PANOFSKY. 1964. The structure of atmospheric turbulence. Wiley.
- MAHRT, L., AND D. H. LENSCHOW. 1976. Growth dynamics of the convective mixed layer. *J. Atmos. Sci.* **33**: 41-51.
- MONIN, A. S., AND A. M. OBUKHOV. 1954. Basic laws of turbulent mixing in the atmosphere near the ground. *J. Akad. Nauk SSSR Geofiz. Inst.* **24**: 163-187.
- MONISMITH, S. G. 1983. The dynamic response of stratified reservoirs to surface shear stress. Ph.D. thesis, Univ. Calif. Berkeley. 304 p. [Also Univ. Calif. Berkeley Hydraulic Eng. Lab. Rep. UCB/HEL-83/05.]
- . 1985. Wind-forced motions in stratified lakes and their effect on mixed-layer shear. *Limnol. Oceanogr.* **30**: 771-783.
- MORTIMER, C. H. 1952. Water movement in lakes during summer stratification. Evidence from the distribution of temperature in Windermere. *Phil. R. Trans. Soc. Lond. Ser. B* **236**: 355-404.
- NIILER, P. P. 1975. Deepening of the wind mixed layer. *J. Mar. Res.* **33**: 405-422.
- PATTERSON, J. C., P. F. HAMBLIN, AND J. IMBERGER. 1984. Classification and dynamic simulation of the vertical density structure of lakes. *Limnol. Oceanogr.* **29**: 845-861.
- POLLARD, R. T., P. B. RHINES, AND R. O. THOMPSON. 1973. The deepening of the wind-mixed layer. *Geophys. Fluid Dyn.* **3**: 381-404.
- RAYNER, K. N. 1980. Diurnal energetics of a reservoir surface layer. M.S. thesis, Univ. Western Australia. 227 p. [Also Univ. W. Aust. Environ. Dyn. Rep. ED-80-005.]
- SHAY, T. J., AND M. C. GREGG. 1984. Turbulence in an oceanic convective mixed layer—corrigendum. *Nature* **311**: 84.
- SHERMAN, F. S., J. IMBERGER, AND G. M. CORCOS. 1978. Turbulence and mixing in stably stratified waters. *Annu. Rev. Fluid Mech.* **10**: 267-288.
- SPIGEL, R. H. 1980. Coupling of internal wave motion width entrainment of the density interface of a two-layer lake. *J. Phys. Oceanogr.* **10**: 144-155.
- , AND J. IMBERGER. 1980. The classification of mixed layer dynamics in lakes of small to medium size. *J. Phys. Oceanogr.* **10**: 1104-1121.
- STRUß, T. 1983. The response of a small lake to atmospheric forcing during fall cooling. Ph.D. thesis, Univ. California, Davis. 288 p.
- THERRY, G., AND P. LACARRÈRE. 1983. Improving the eddy kinetic energy model for planetary boundary layer description. *Boundary-Layer Meteorol.* **25**: 63-88.
- THOMPSON, R. O., AND J. IMBERGER. 1980. Response of a numerical model of a stratified lake to wind stress, p. 562-570. In *Stratified flows. Proc. 2nd Int. Symp. Trondheim*, v. 1.
- THORPE, S. A. 1973. Turbulence in stratified fluids: A review of laboratory experiments. *Boundary-Layer Meteorol.* **5**: 95-119.
- . 1977. Turbulence and mixing in a Scottish loch. *Phil. Trans. R. Soc. Lond. Ser. A* **286**: 125-181.
- . 1984. On the determination of K_z in the near-surface ocean from acoustic measurements of bubbles. *J. Phys. Oceanogr.* **14**: 855-863.
- , AND J. M. BRUBAKER. 1983. Observations of sound reflections by temperature microstructure. *Limnol. Oceanogr.* **28**: 601-613.
- WEDDERBURN, E. M. 1912. Temperature observations in Loch Earn with a further contribution to the hydrocynamical theory of temperature seiches. *Trans. R. Soc. Edinburgh* **48**: 629-695.
- WILLIS, G. E., AND J. W. DEARDORFF. 1974. A laboratory model of the unstable planetary boundary layer. *J. Atmos. Sci.* **31**: 1297-1307.
- ZEMAN, O., AND H. TENNEKES. 1977. Parameterization of the turbulent energy budget at the top of the daytime atmospheric boundary layer. *J. Atmos. Sci.* **34**: 111-123.
- ZILITINKEVICH, S. S. 1975. Comments on "A model for the dynamics of the inversion above a convective boundary layer." *J. Atmos. Sci.* **32**: 991-992.

Submitted: 8 May 1984

Accepted: 28 January 1985